IFN-γ, a cytokine secreted by activated T cells, natural killer cells and natural killer T cells, has immunomodulatory effects on several cell types. IFN-γ is one of the major cytokines responsible for the activation of macrophages that mediate non-specific, cell-mediated host defenses. To gain a better understanding of the pathological role of IFN-γ in specific mycobacterial granuloma formation, IFN-γ gene-deficient mice (BALB/c and C57BL/6) were produced. The IFN-γ gene in embryonic stem cells was disrupted by inserting the β-galactosidase gene (*lac*Z) and the neomycin resistance gene (*neo*) at the translation initiation site in exon 1 by homologous recombination[2]. Six-week-old IFN-γ-deficient and wild-type mice were inoculated with $10^{3-7}$ tubercle bacilli of various strains of *M. tuberculosis* (Kurono, H37Rv, and H37Ra) and BCG Pasteur aerially. The mice were examined seven weeks later for pulmonary granuloma formation. The relatively avirulent BCG Pasteur and H37Ra strains induced granulomas in the lungs, spleen and liver of IFN-γ-deficient mice. The granulomas consisted of epithelioid macrophages and Langhans-type multinucleated giant cells with central necrosis during long-term observations (9 months). The virulent Kurono and H37Rv strains induced disseminated abscesses but not granulomas in various organs of IFN-γ-deficient mice and Mac-3-positive macrophages were not detected in the abscess lesions. These results suggest that IFN-γ may be responsible primarily for macrophage activation and that other factors may be involved in the granuloma formation mechanism[3].

### 4. Roles of TNF-α in murine tuberculosis

TNF-α is a cytokine with various activities that are induced by activated macrophages through signal transduction at two distinct receptors. It mediates inflammation and produces protective immunity against bacterial, parasitic, and viral infections, and is thought to play a significant role in the pathogenesis of various diseases, including cancer. Of the several cytokines associated with the pathogenesis of tuberculosis, including IL-12 and IFN-γ, TNF-α is thought to be responsible for protection against the development of the disease. Kindler et al. showed that depletion of TNF-α using polyclonal antibodies blocked granuloma formation and impaired the ability to localize infection with BCG in mice[4]. Infusion of TNF-α has been shown to increase resistance against *M. tuberculosis* and *M. avium* in mice[5]. Clearly, there are conflicting data with respect to the role of TNF-α in granuloma formation. To study the role of TNF-α in mycobacterial infection, we generated TNF-α-knockout mice, in which the third and fourth exons of the TNF-α gene were disrupted. The C57BL/6 KO mice were infected with the virulent *M. tuberculosis* strain Kurono or the relatively avirulent bacillus BCG Pasteur ($10^6$ CFU), by IES as described previously. The major organs were removed at weekly intervals, and morphologic observation, assay of IL-1, IL-12, IFN-γ, and inducible nitric oxide synthase mRNA expression, and colony counts in the lungs and spleen were performed. Peritoneal and alveolar macrophages from BCG- and H37Rv strain-treated mice produced significant levels of nitric oxide after stimulation *in vitro*. The formation of abscesses was seen only in the Kurono-treated groups, and these abscesses contained large numbers of mycobacteria. The administration of recombinant TNF-α significantly ameliorated the mycobacterial lesions. IFN-γ mRNA was expressed significantly in virulent H37Rv-treated groups with time, and the number of mycobacterial colonies per unit weight increased markedly with time. Nitric oxide production was not observed in H37Rv-treated groups but was seen in BCG-treated groups. We concluded that TNF-α played an important role in protective immunity against virulent mycobacteria. Because avirulent mycobacteria did not induce granulomas in TNF-α-KO mice. TNF-α played an indirect role in granuloma formation[6].

### 5. Other cytokines

IL-12, IL-18, IL-4, and IL-1, as well as IFN-γ and TNF-α, play important roles in protective immunity against mycobacterial infection. IL-12-, IL-18-, IL-4-, and IL-1-KO mice did not die when they were infected with the virulent Kurono strain via an airborne route in our experiments[7)~9)]. It is thought that these cytokines are not necessary for protection against mycobacterial infection or the functions of these cytokines are compensated for by other cytokines. If we rank the cytokines in terms of their roles in mycobacterial infection, we can construct a cytokine hierarchy in murine tuberculosis, as shown in Fig.

### 6. Clinical implications

I have presented some important findings from experimental murine tuberculosis. What is the clinical relevance of murine tuberculosis? I have reported previously that serum IFN-γ levels are significantly low in patients with advanced, and active TB[10] and it has also been reported that people with IFN-γ receptor deficiency are susceptible to *M. tuberculosis*[11]. On the other hand, humanized anti-TNF-α neutralizing monoclonal antibody is given to patients with rheumatoid

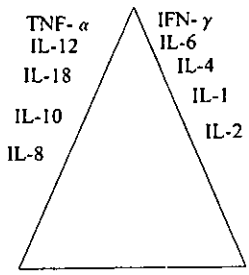


**Fig.** Cytokine hierarchy in tuberculosis

arthritis and Crohn's disease whose serum TNF-α levels are low [12] and these patients develop readily tuberculosis. Thus, it is meaningful to study murine tuberculosis for the insights into clinical tuberculosis.

## 7. Conclusion

I briefly reviewed the roles of cytokines in experimental mycobacterial infection with special emphasis on the roles of IFN-γ and TNF-α. IFN-γ and TNF-α are the 'grand champions' among the cytokines involved in mycobacterial infection. Therefore, it is very important to investigate their roles and regulatory factors for IFN-γ and TNF-α in early-phase mycobacterial infection in more detail, so that tuberculosis can be diagnosed and treated as early as possible.

## 8. Acknowledgments

The author expresses his appreciation to Prof. Yoichiro Iwakura (The Institute of Medical Sciences, University of Tokyo), Prof. Shizuo Akira (Osaka University), Dr. Kenji Sekikawa (National Institute of Animal Health), and the staff in his laboratory for their help and encouragement. Part of this work was supported by an International Collaborative Study Grant from the Ministry of Health, Wealth and Labor, Japan.

## References

1) Sugawara I, Yamada H, Otomo K, et al.: Optimal conditions for establishment of experimental tuberculosis model using an automated inhalation exposure apparatus and its application. Kekkaku. 2000 ; 75 : 463–469.

2) Tagawa Y, Sekikawa K, Iwakura Y: Suppression of Con A-induced hepatitis in IFN-γ -/-, but not in TNF-α -/- mice: role for IFN-γ in activating apoptosis in hepatocytes. J Immunol. 1997 ; 159 : 1418–1428.

3) Sugawara I, Yamada H, Otomo K, et al.: Granulomas in IFN-gamma gene-disrupted mice are inducible by avirulent *Mycobacterium*, but not by virulent *Mycobacterium*. J Med Microbiol. 1998 ; 47 : 871–877.

4) Kindler V, Sappino A-P, Grau GE, et al.: The inducing role of tumor necrosis factor in the development of bactericidal granulomas during BCG infection. Cell. 1989 ; 56 : 731–740.

5) Bermudez LE, Stevens P, Kolonoski P, et al.: Treatment of *Mycobacterium avium* complex infection in mice with recombinant human IL-2 and tumor necrosis factor. J Immunol. 1989 ; 143 : 2996–3000.

6) Kaneko H, Yamada H, Mizuno S, et al.: Role of tumor necrosis factor-α in Mycobacterium-induced granuloma formation in tumor necrosis factor-α -deficient mice. Lab Invest. 1999 ; 79 : 379–386.

7) Sugawara I, Yamada H, Kaneko H, et al.: Role of IL-18 in mycobacterial infection in IL-18-gene-disrupted mice. Infect Immune. 1999 ; 67 : 2585–2589.

8) Sugawara I, Yamada H, Mizuno S, et al.: IL-4 is required for defense against mycobacterial infection. Microbial Immunol. 2000 ; 44 : 971–979.

9) Yamada H, Mizuno S, Horai R, et al.: Protective role of IL-1 in mycobacterial infection in IL-1 α / β double-knockout mice. Lab Invest. 2000 ; 80 : 759–767.

10) Jitsukawa T, Nakajima S, Sugawara I, et al.: Characterization of murine monoclonal antibodies to human IFN-γ and their application for sandwich ELISA. Microbiol Immunol. 1987 ; 31 : 809–820.

11) Jouanguy E, Lamhamedi-Cherradi S, Altare F, et al.: Partial interferon-gamma receptor 1 deficiency in a child with tuberculoid BCG infection and a sibling with clinical tuberculosis. J Clin Invest. 1997 ; 11 : 2658–2664.

12) Keane J, Gershon S, Wise RP, et al.: Tuberculosis associated with infliximab, a tumor necrosis factor-alpha-neutralizing agent. N Engl J Med. 2001 ; 345 : 1098–1103.

**Memorial Lecture by the Imamura Award Winner, 2002**

# STUDY ON THE ROLES OF CYTOKINES INVOLVED IN MYCOBACTERIAL INFECTION

Isamu SUGAWARA

**Abstract** The roles of various cytokines in early-phase mycobacterial infection were investigated utilizing murine tuberculosis models. Among them, IFN-$\gamma$ and TNF-$\alpha$ are very important in protective immunity against mycobacterial infection. This finding is closely associated with human tuberculosis. It is reported that persons with IFN-$\gamma$ receptor 1 deficiency and patients with rheumatoid arthritis and Crohn's disease are susceptible to *Mycobacterium tuberculosis*. It is expected that a novel immunotherapy and a diagnostic method of tuberculosis are developed by clarifying roles of various cytokines immunologically in early-phase mycobacterial infection.

**Key words**: Cytokine, Aerosol infection, *M. tuberculosis*, IFN-$\gamma$, TNF-$\alpha$

Research Institute of Tuberculosis, Japan Anti-Tuberculosis Association

Correspondence to : Isamu Sugawara, Department of Molecular Pathology, Research Institute of Tuberculosis, Japan Anti-Tuberculosis Association, 3−1−24, Matsuyama, Kiyose-shi, Tokyo 204−8533 Japan. (E-mail: sugawara@jata.or.jp)

J. Med. Microbiol. — Vol. 51 (2002), 131–137

ISSN 0022-2615

MICROBIAL PATHOGENICITY

# Pulmonary granulomas of guinea pigs induced by inhalation exposure of heat-treated BCG Pasteur, purified trehalose dimycolate and methyl ketomycolate

I. SUGAWARA, T. UDAGAWA, S. C. HUA, M. REZA-GHOLIZADEH, K. OTOMO, Y. SAITO* and H. YAMADA

*Department of Molecular Pathology, Research Institute of Tuberculosis, Japan Anti-Tuberculosis Association, 3-1-24 Matsuyama, Kiyose, Tokyo 204-0022, and *4th Department of Internal Medicine, Nippon Medical School, Sendagi, Bunkyo-ku, Tokyo 113-8603, Japan*

**This study was designed to determine the identity of granulomatogenic substances in *Mycobacterium bovis* BCG Pasteur. When heat-treated BCG Pasteur bacilli were introduced into the lungs of guinea-pigs by an inhalation exposure apparatus, pulmonary granulomas without necrosis developed. Furthermore, when four kinds of mycolates derived from *M. tuberculosis* Aoyama B strain were introduced into the lungs by the same method, only trehalose 6,6′-dimycolate (TDM) and methyl ketomycolate induced pulmonary granulomas without central necrosis. The pulmonary granulomas consisted of epithelioid macrophages and lymphocytes. When a mixture of TDM and anti-TDM antibody was introduced into the lungs, development of granulomatous lesions was reduced. These data indicate that TDM and methyl ketomycolate are potent granulomatogenic reagents.**

## Introduction

Chronic mycobacterial infection is characterised by granuloma formation with central caseous necrosis [1]. It is known that trehalose 6,6′-dimycolate (TDM; cord factor) derived from *Mycobacterium tuberculosis* induces granulomas when injected intravenously in adjuvant preparations [2–6]. As human mycobacterial granulomas are induced by an airborne route, it is meaningful to examine whether granulomas can be induced in experimental animals by this route. Also, there are many mycolic acid derivatives in the cell walls of mycobacteria and it is important to find other substances with granulomatogenic activity to understand the pathogenesis of tuberculosis.

An inhalation exposure system was established previously to induce pulmonary granulomas efficiently [7–9]. The present experiments with this system were designed to examine whether killed mycobacteria and TDM could induce granulomas aerially. At the same time, the granuloma-forming activity of mycolic acid derivatives other than TDM was also examined.

Received 2 April 2001; revised version accepted 27 July 2001.
Corresponding author: Dr I. Sugawara (sugawara@jata.or.jp).

## Materials and methods

### *Animals*

Hartley female guinea-pigs (6-week-old) were purchased from Nippon SLC, Hamamatsu, Japan. They were kept in sterile, filter-topped cages and given sterile food and sterile, distilled water in a specific pathogen-free room.

### *Mycobacterial strain and reagents*

*M. bovis* BCG Pasteur bacilli (ATCC 27289) were grown in 7H9 medium (Difco) to mid-log phase. They were then heat-treated at 95°C for 30 min in double-distilled water and autoclaved at 121°C for 30 min; then the treated strain was filtered with a 4-$\mu$m pore-size membrane filter (Millipore) before use to ensure even dispersal. TDM, methyl methoxymycolate methyl ketomycolate and methyl $\alpha$-mycolate were purchased from Nacalai Tesque, Kyoto, Japan. They were extracted from *M. tuberculosis* Aoyama B strain with chloroform/methanol and developed on a thin-layer

plate of silica gel (Analtech, Newark, DE, USA) with the solvent system of chloroform/methanol/acetone/acetic acid. Each was recovered with chloroform/methanol, and the purification was repeated until a single spot was achieved by thin-layer chromatography. The structures of the four mycolates are illustrated in Fig. 1.

Rabbit anti-TDM polyclonal antibody was supplied by Nacalai Tesque. The anti-TDM antibody was generated by immunising New Zealand White rabbits five times with purified TDM in Freund's adjuvant.

### *Inhalation exposure experiments*

Guinea-pigs were exposed to heat-treated BCG Pasteur autoclaved BCG Pasteur or mycolic acid derivative suspensions aerially by placing them in the exposure chamber of an inhalation exposure apparatus (Model 099CA4212; Glas-Col, Terre Haute, IN, USA). Five guinea-pigs were used for each treatment with BCG and three for each mycolic acid treatment. The nebuliser compartment was filled with 5 ml of a suspension containing $10^7$ dead BCG Pasteur organisms or 1–5 mg of mycolic acid derivatives. In several experiments, 1 mg of rabbit anti-TDM polyclonal antibody was added to 1 mg of TDM 30 min before inhalation exposure.

### *Histopathology*

All guinea-pigs were killed 7 weeks after the inhalation exposure experiments. For light microscopy, sections cut from paraffin blocks containing lung, liver, lymph nodes and spleen tissues from the guinea-pigs were stained with haematoxylin and eosin. For electron microscopy, fresh lung tissue was cut into pieces, fixed with glutaraldehyde 2.5%, post-fixed with osmium tetroxide 1%, and embedded in Spurr's low-viscosity embedding medium [9, 10].

### *Immunohistochemistry*

Immunohistochemistry was performed with avidin-biotin complex (ABC) peroxidase (PO) [11, 12]. Anti-*M. bovis* BCG antibody (Dakopatts, Copenhagen, Denmark) was used at a final concentration of 0.1 $\mu$g/ml. This antibody recognises cell wall components of *M. bovis*. Lung tissue infected with live BCG was used as a positive control.

### *DNA extraction and PCR*

PCR was used to evaluate the degree of DNA destruction by heat treatment and autoclaving. *M. bovis* BCG Pasteur was boiled and then autoclaved in double-distlled water and the DNA was purified with a Nucleon II DNA extraction kit (Scotlab, Coatbridge, Scotland) [11, 13]. DNA was similarly extracted from pulmonary lesions. Whitish nodular lesions of the lung were obtained for DNA extraction [11].

Primers corresponding to portions of the *M. tuberculosis IS*6110 and 19-kDa antigen DNA sequences were synthesised on a 381 DNA synthesiser (Perkin-Elmer Cetus, Norwalk, CT, USA). The samples were

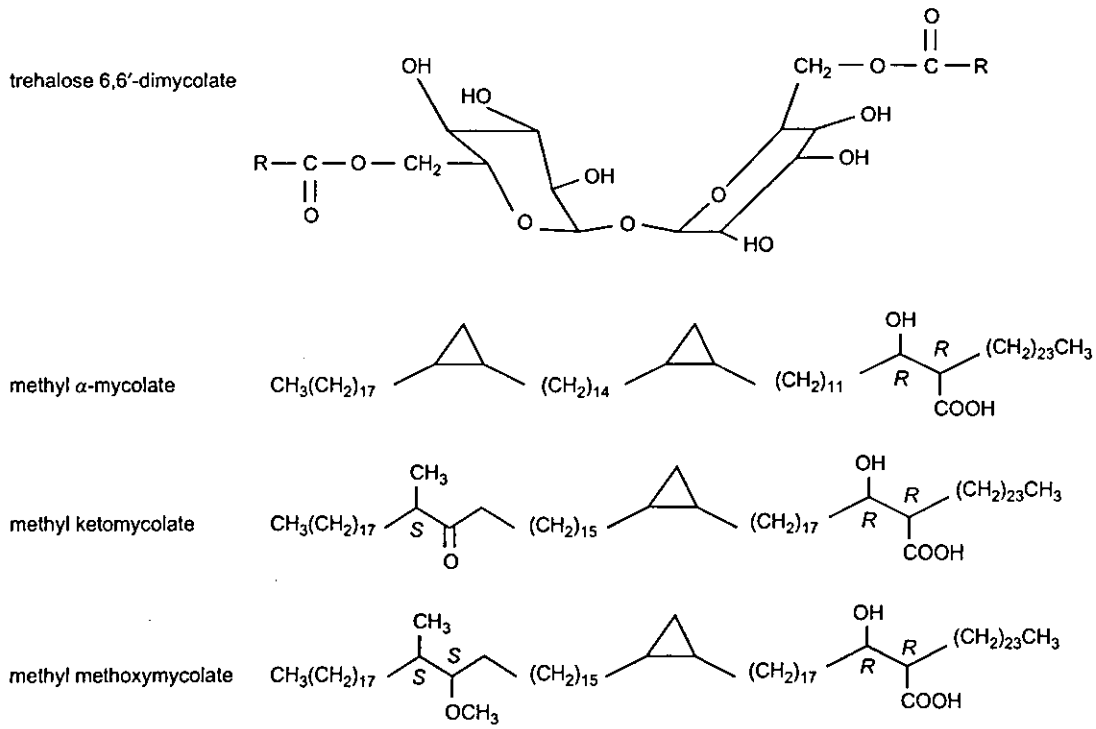


**Fig. 1.** Chemical structures of four mycolate derivatives.


**Fig. 2.** Representative histology of pulmonary tissues exposed to heat-treated BCG Pasteur (**a**), TDM (**b**), methyl ketomycolate (**c**) and a mixture of TDM and anti-TDM antibody (**d**). Haematoxylin and eosin stain, ×85. Granulomas that consist of epithelioid macrophages and lymphocytes are recognised in **a**, **b**, and **c** but not in **d**.

amplified through 35 cycles in a programmable thermal cycler (Perkin-Elmer Cetus) with a three-step cycle of denaturation for 2 min at 94°C, annealing for 1.75 min at 60°C and extension for 2.5 min at 72°C. The amplification products (541 and 320 bp) were analysed by electrophoresis through an agarose 2.0% gel with a Tris-borate-EDTA buffer system and visualised by fluorescence after ethidium bromide staining [7, 9].

### *Statistical analysis*

All values were expressed as means and SEM and compared by Student's *t* test. For all statistical analyses, differences at $p < 0.01$ were considered significant.

## Results

### *Histopathology of the lungs*

When heat-treated BCG Pasteur was administered aerially, pulmonary granulomatous lesions without central necrosis developed in all five guinea-pigs (Fig. 2a), but autoclaved BCG Pasteur did not induce pulmonary granulomatous lesions. Of the four mycolate derivatives, TDM, methyl ketomycolate, methyl mathoxymycolate and methyl $\alpha$-mycolate, only TDM and methyl ketomycolate induced pulmonary granulomatous lesions ($p < 0.01$) (Figs. 2b and c). The granulomatous lesions consisted of lymphocytes and epithelioid macrophages. When the mixture of TDM and anti-TDM antibody was introduced aerially,

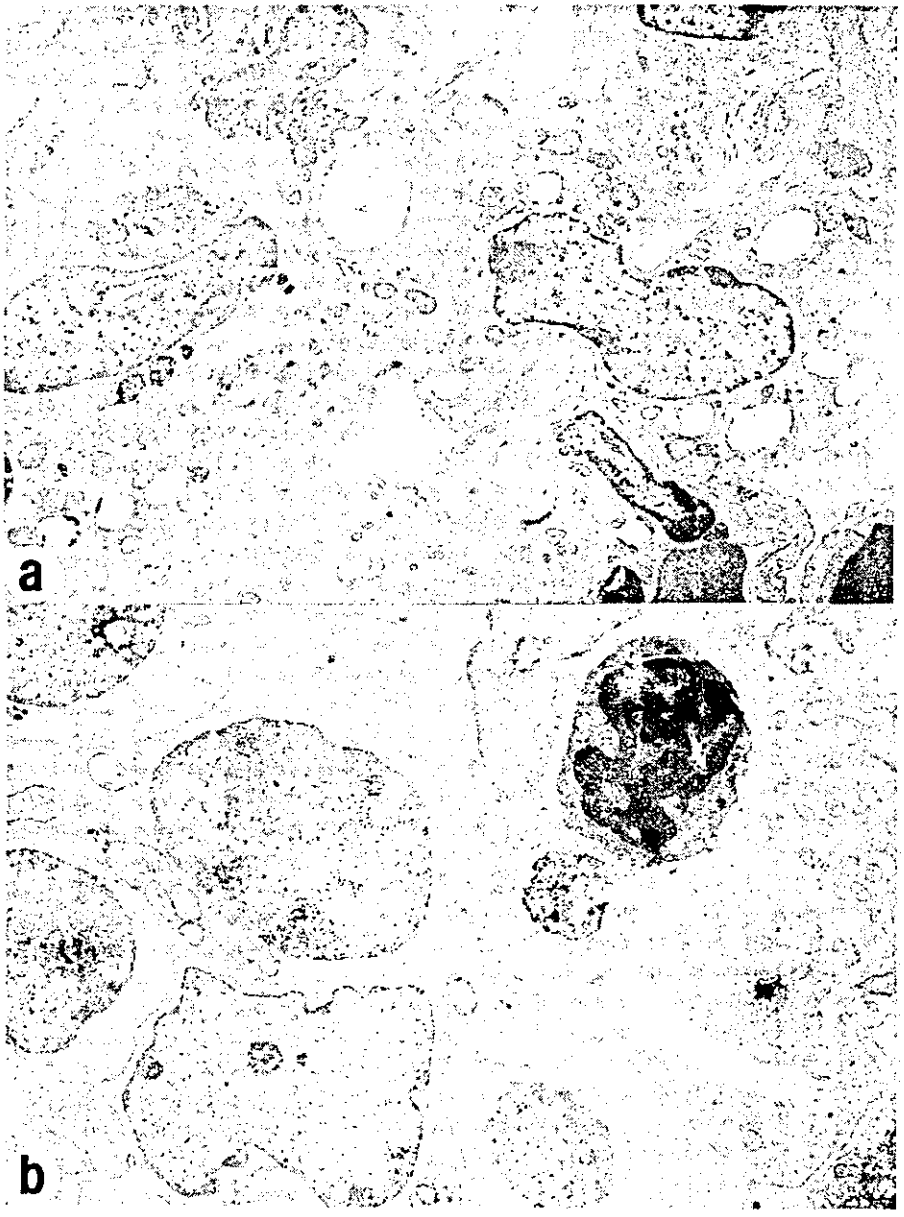


**Fig. 3.** Electron micrographs of pulmonary granulomas from a BALB/c mouse exposed to aerosols of (a) TDM (×4900) or (b) methyl ketomycolate (×5900). Several epithelioid macrophages and lymphocytes are shown.


**Fig. 4.** Immunohistochemistry of pulmonary granulomas immunostained with anti-BCG antibody (×85; ABC-PO method, counterstained with haematoxylin). BALB/c mice were exposed to aerosols containing (**a**) heat-treated BCG Pasteur bacilli; (**b**) TDM, (**c**) methyl ketomycolate and (**d**) live BCG Pasteur bacilli. Only epithelioid macrophages from mice exposed to aerosols of live BCG Pasteur were immunostained intensely with anti-BCG (**d**).

granulomas were hardly recognised (Fig. 2d). Langhans-type multinucleate giant cells were not observed.

Similar pathology was observed by electron microscopy. Discrete and small granuloma formation was noted in both TDM- and methyl ketomycolate-treated lung tissues. The granulomatous lesions consisted of epithelioid macrophages of varying sizes, lymphocytes and small vessels. No eosinophil, basophil or plasma cells were observed in these lesions (Fig. 3a).

Immunohistochemically, the antigens (cell wall components) recognised by anti-BCG antibody were present in epithelioid macrophages of the granulomatous lesions when live BCG Pasteur was used (Fig. 4d), but not in epithelioid macrophages when heat- and autoclave-treated BCG Pasteur, TDM and methyl ketomycolate were introduced into the lungs of guinea-pigs (Fig. 4a, b and c).

### *PCR*

Large DNA fragments were not obtained from the heat-treated and autoclaved BCG Pasteur. *M. tuberculosis*-specific 19-kDa antigen gene fragments and IS*6110*-related DNA fragments were detected by PCR in live BCG Pasteur, but not detected in heat-treated and autoclaved *M. bovis* BCG (Fig. 5).

## Discussion

Granulomas were induced successfully in the lungs when killed BCG Pasteur bacilli, purified TDM and methyl ketomycolate were introduced aerially in an inhalation exposure apparatus. Intravenous injection of TDM and adjuvant is the preferred method for inducing granulomas efficiently [2, 5, 6]. This study examined whether TDM as one of the causative agents of *Mycobacterium*-induced granulomas induces similar granulomatous lesions after inhalation exposure.

TDM is a well-known, toxic glycolipid in *M. tuberculosis*. It is also reported that TDM derived from *Nocardia* and *Rhodococcus* possesses granuloma-forming activity [5, 13]. In the present study, methyl ketomycolate induced pulmonary granulomas, but methyl $\alpha$-mycolate and methyl methoxymycolate did not. The molecular basis for the similar granuloma-inducing activity of TDM and methyl ketomycolate is unknown because there is little structural similarity between them. Further study will be required to clarify this discrepancy.

Anti-BCG antibody reacted with granulomas induced by live *M. bovis* BCG Pasteur but did not react with granulomas induced by heat-treated and autoclaved BCG Pasteur. Mycobacterial cell wall components are destroyed by heat treatment and autoclaving. This may explain non-reactivity with granulomas induced by heat-treated and autoclaved BCG. The anti-BCG antibody also did not react with TDM and methyl ketomycolate, as evidenced by the absence of immunostaining in granulomas induced by them.

It is evident that mycobacterial cell wall components induce pulmonary granulomas because *Mycobacterium*-specific DNA fragments were not detected in granulomatous lesions induced by heat-treated BCG Pasteur as assessed by PCR. Autoclaved BCG Pasteur and heat-treated BCG Pasteur did not contain mycobacterial DNA as assessed by gel electrophoresis. Pulmonary granulomatous lesions without central necrosis developed from the introduction of heat-treated BCG Pasteur, but autoclaved BCG Pasteur did not induce pulmonary granulomatous lesions. Heat treatment at 95°C for 30 min does not affect granulomatogenic substances, but autoclaving at 121°C for 30 min may destroy cell wall components completely. Heat- treated H37Rv also induced pulmonary granulomas without necrosis (data not shown).

TDM is a potent granulomatogenic substance reported

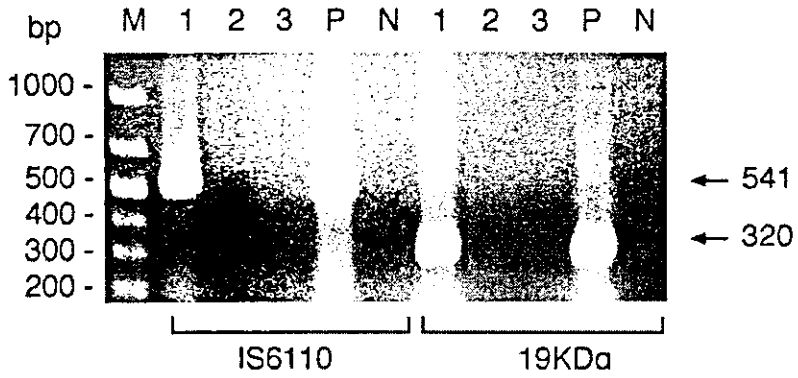


**Fig. 5.** PCR products of 19-kDa antigen-specific and IS*6110* amplification separated in agarose 2% gel. **M**, size marker; lane **1**, DNA from BCG Pasteur bacilli; **2**, DNA from heat-treated BCG Pasteur bacilli; **3**, DNA from autoclaved BCG Pasteur bacilli; **P**, DNA from *M. tuberculosis* H37Rv; **N**, negative control (no DNA). The 19-kDa antigen-specific and IS*6110*-specific amplified bands (320 bp and 541 bp) are not present in lanes 2 and 3.

by many studies [2–6]. When antibody to TDM was added to TDM before exposure of guinea-pigs to aerosols, the mixture abolished granuloma formation significantly. This antibody blocked the granulomatogenic action by binding to TDM. Methyl ketomycolate was also granolomatogenic by inhalation exposure. Thus, methyl ketomycolate is a granulomatogenic candidate that may be important in the development of human tuberculosis.

The granulomas induced by heat-treated BCG Pasteur, TDM and methyl ketomycolate consist of lymphocytes and epithelioid macrophages. This granuloma is different from hypersensitivity pneumonitis, which consists of plasma cells and basophils as well as lymphocytes and epithelioid macrophages [14, 15]. It is reported that TDM induces foreign body- and hypersensitivity-type granulomas in mice [16]. According to these published criteria, the granulomas formed in the present study were of the foreign bodytype.

In summary, heat-treated BCG Pasteur, TDM and methyl ketomycolate were shown to induce pulmonary granulomas after inhalation exposure. TDM and methyl ketomycolate may play an important role in the pathogenesis of tuberculosis.

This study was supported in part by an International Collaborative Study Grant awarded to I. S. from the Ministry of Health, Labor and Welfare, Japan. We thank Professor Emeritus I. Yano for useful suggestions. Part of this work was presented at the Annual Meeting of the Japanese Society of Sarcoidosis and related granulomatous diseases, Oita, Japan, in 2000.

## References

1. Garay SM. Pulmonary tuberculosis. In: Rom WN, Garay SM (eds) Tuberculosis. Boston, Little, Brown and Company. 1996: 373–412.
2. Behling CA, Perez RL, Kidd MR, Staton GW, Hunter RL. Induction of pulmonary granulomas, macrophage procoagulant activity, and tumor necrosis factor-alpha by trehalose glycolipids. *Ann Clin Lab Sci* 1993; **23**: 256–266.
3. Yamamoto K, Kakinuma M, Kato K, Okuyama H, Azuma I. Relationship of anti- tuberculous protection to lung granuloma produced by intravenous injection of synthetic 6-O-mycoloyl-N-acetylmuramyl-L-alanyl-D-isoglutamine with or without specific antigens. *Immunology* 1980; **40**: 557–564.
4. Bekierkunst A, Levij IS, Yarkoni E, Vilkas E, Adam A, Lederer E. Granuloma formation induced in mice by chemically defined mycobacterial fractions. *J Bacteriol* 1969; **100**: 95–102.
5. Natsuhara Y, Yoshinaga J, Shogaki T *et al.* Granuloma-forming activity and antitumor activity of newly isolated mycolyl glycolipid from *Rhodococcus terrae* 70012 (Rt. GM-2). *Microbiol Immunol* 1990; **34**: 45–53.
6. Sakurai T, Saiki I, Ishida H, Takeda K, Azuma I. Lethal toxicity and adjuvant activities of synthetic TDM and its related compounds in mice. *Vaccine* 1989; **7**: 269–274.
7. Sugawara I, Yamada H, Kaneko H, Mizuno S, Takeda K, Akira S. Role of interleukin-18 in mycobacterial infection in IL-18-gene disrupted mice. *Infect Immun* 1999; **67**: 2585–2589.
8. Sugawara I, Yamada H, Mizuno S, Iwakura Y. IL-4 is required for defense against mycobacterial infection. *Microbiol Immunol* 2000; **44**: 971–979.
9. Yamada H, Mizumo S, Horai R, Iwakura Y, Sugawara I. Protective role of interleukin-1 in mycobacterial infection in interleukin-1 alpha/beta double-knockout mice. *Lab Invest* 2000; **80**: 759–767.
10. Nakamura H, Morishita Y, Sugawara I *et al.* Ultrastructural localization of antigens recognized by 5D-4 monoclonal antibody reactive with islets of Langerhans. *J Clin Electron Microsc* 1990; **23**: 393–398.
11. Sugawara I, Yamada H, Kazumi Y *et al.* Induction of granulomas in interferon-γ gene-disrupted mice by avirulent but not by virulent strains of *Mycobacterium tuberculosis*. *J Med Microbiol* 1998; **47**: 871–877.
12. Hsu S-M, Raine L, Fanger H. Use of avidin-biotin-peroxidase complex (ABC) in immunoperoxidase techniques: a comparison between ABC and unlabeled antibody (PAP) procedures. *J Histochem Cytochem* 1981; **29**: 577–580.
13. Han Y, Kawada N, Yano I. Granuloma formation and in vitro macrophage activation in mice by mycoloyl glycolipids from *Nocardia asteroides* and related taxa. *Osaka City Med J* 1998; **44**: 201–217.
14. Schuyler M, Gott K, Haley P. Experimental murine hypersensitivity pneumonitis. *Cell Immunol* 1991; **136**: 303–317.
15. Takizawa H, Ohta K, Horiuchi T *et al.* Hypersensitivity pneumonitis in athymic nude mice. Additional evidence of T cell dependency. *Am Rev Respir Dis* 1992; **146**: 479–484.
16. Yamagami H, Matsumoto T, Fujiwara N *et al.* Trehalose 6,6'-dimycolate (cord factor) of *Mycobacterium tuberculosis* induces foreign-body- and hypersensitivity-type granulomas in mice. *Infect Immun* 2001; **69**: 810–815.

CONCISE COMMUNICATION

# Genetic Basis of Patients with Bacille Calmette-Guérin Osteomyelitis in Japan: Identification of Dominant Partial Interferon-γ Receptor 1 Deficiency as a Predominant Type

**Yuka Sasaki,[1] Akihiko Nomura,[1] Koichi Kusuhara,[1] Hidetoshi Takada,[1] Saifuddin Ahmed,[1] Kaoru Obinata,[2] Keisuke Hamada,[3] Yuri Okimoto,[4] and Toshiro Hara[1]**

*[1]Department of Pediatrics, Graduate School of Medical Sciences, Kyushu University, Fukuoka, [2]Department of Pediatrics, Koshigaya City Hospital, Saitama, [3]Department of Pediatrics, Miyazaki Prefectural Hospital, Miyazaki, and [4]Department of Hematology/Oncology, Chiba Children's Hospital, Chiba, Japan*

**Interferon (IFN)-γ-mediated immunity plays an important role in host defense against intracellular pathogens, especially mycobacteria. Six Japanese children with bacille Calmette-Guérin (BCG) osteomyelitis were evaluated (1 disseminated, 3 multiple, and 2 solitary types) for mutations of genes involved in interleukin-12-dependent, IFN-γ-mediated immunity. Heterozygous small deletions with frameshift (818del4 and 811del4) that are consistent with the diagnosis of partial dominant IFN-γ receptor 1 (IFN-γR1) deficiency were detected in 3 unrelated patients. Expression of IFN-γR1 on monocytes was significantly increased in all 3 patients. Screening of family members with recurrent and disseminated mycobacterial infections found the identical deletion in 1 of the fathers. Antimycobacterial treatment was effective in these patients and resulted in good clinical outcome. This study demonstrated that partial dominant IFN-γR1 deficiency was the most common in Japanese patients who showed predisposition to curable BCG osteomyelitis.**

Bacille Calmette-Guérin (BCG) osteomyelitis is a rare late-onset complication of BCG vaccination. An international survey on the complications of BCG vaccination showed that the incidence of osteomyelitis was 0.89–2.41 and 0.02–0.06 per 1 million among vaccine recipients at ages <1 year and ≥1 year, respectively [1]. Only a few cases without any immunodeficiency have been reported annually in Japan, even though before age 3 years >90% of Japanese children receive multipuncture percutaneous inoculation with BCG Tokyo 172 strain, the least virulent substrain.

Recently, mutations in *IFNGR1* [2–4], *IFNGR2* [5, 6], *IL12B* [7], *IL12RB1* [8–10], and the signal transducer and activator of transcription-1 gene *(STAT-1)* [11] have been identified in humans who manifest higher susceptibility to BCG, nontuberculous mycobacteria, *Mycobacterium tuberculosis,* other intracellular microbes (e.g., *Salmonella*), *Listeria monocytogenes* [12], and certain viruses [13] in the absence of a known immunodeficiency. In this study, we investigated 6 Japanese children with BCG osteomyelitis for defects in interleukin (IL)-12-dependent, interferon (IFN)-γ-mediated immunity.

## Patients and Methods

### Patients

Six unrelated patients with curable BCG osteomyelitis were investigated (table 1). All had been vaccinated with BCG in the upper arm. Unaffected family members of the 3 patients with *IFNGR1* mutations were also analyzed.

*Patient 1.* The patient developed lymphadenitis 2 months after BCG vaccination. Nine months after inoculation, she had papules and abscesses over the limbs and trunk. Radiographic studies showed multiple destructive lesions over 17 bones. Cultures from bone biopsy specimens grew *M. bovis.* She was treated with isoniazid, rifampicin, and streptomycin and showed slow improvement. Eighteen months after her initial presentation, she had recurrent osteomyelitis in her right femur. She is now recovering with antimycobacterial therapy.

*Patient 2.* The patient presented with prolonged intermittent fever, lymphadenitis, and liver dysfunction 2 months after BCG inoculation. Antibiotics were not effective, but administration of isoniazid for 9 months improved his condition. Four months after discontinuation of isoniazid, he developed osteomyelitis at the left humerus and left calcaneus and was again treated with isoniazid. At age 3 years, he developed osteomyelitis of the left clavicle that healed with isoniazid therapy. Specimens were not processed or were not available for mycobacterial culture in each episode. His father (patient 2') also showed increased susceptibility to mycobacteria.

Received 19 July 2001; revised 4 November 2001; electronically published 14 February 2002.

Informed consent was obtained from patients, family members, or parents. Experimentation guidelines of the authors' institutions were followed in the conduct of this research.

Financial support: Ministry of Education, Culture, Sports, Science, and Technology of Japan (grant 12204009).

Reprints or correspondence: Dr. Yuka Sasaki, Dept. of Pediatrics, Graduate School of Medical Sciences, Kyushu University, 3-1-1 Maidashi, Higashi-ku, Fukuoka 812-8582, Japan (yuka@pediatr.med.kyushu-u.ac.jp).

**The Journal of Infectious Diseases 2002;185:706–9**

0022-1899/2002/18505-0020$02.00

**Table 1.** Characteristics of patients with bacille Calmette-Guérin (BCG) osteomyelitis.

| Patient[a] | Age at BCG inoculation | Osteomyelitis | | | Other affected organs | Immunologic studies | | | |
|---|---|---|---|---|---|---|---|---|---|
| | | Age at onset | Type | Histology | | WBCs/μL | Lymphocytes/μL | CD3 cells, % | CD4:CD8 |
| 1 (AII-1) | 8 months | 1 year 5 months | Multiple, recurrent | Granuloma | Skin, lymph node | 29,600 | 7104 | 56.6 | 3.0 |
| 2 (BIII-3) | 4 months | 1 year 7 months | Multiple, recurrent | Inflammation | Lymph node | 24,200 | 6098 | 51.0 | 3.3 |
| 3 (CII-1) | 1 year 7 months | 2 years 2 months | Multiple | Inflammation | None | 5300 | 3657 | 40.7 | 3.0 |
| 4 | 4 months | 1 year 5 months | Solitary | ND | None | 10,560 | 4224 | 52.0 | 1.7 |
| 5 | 3 months | 1 year 9 months | Solitary | Granuloma | None | 7220 | 4115 | ND | ND |
| 6 | 11 months | 1 year 4 months | Multiple | Granuloma | Skin, muscle | 7600 | 3724 | 60.2 | 1.1 |
| 2′ (BII-1) | ND | 31 years | Solitary[b] | Granuloma | Lymph node[c] | — | — | — | — |

NOTE. ND, not determined; WBC, white blood cell.
[a] Pedigree designations from figure 1 are indicated in parentheses for patients with *IFNGR1* mutations.
[b] Due to *Mycobacterium avium* complex.
[c] Due to *Mycobacterium tuberculosis*.

He had *M. tuberculosis* lymphadenitis of the neck at age 3 years and bilateral inguinal lymphadenitis, which were shown by biopsy at age 23 years to be granulomatous lesions. At age 31, patient 2′ developed *M. avium* osteomyelitis in his ribs, which subsided with antimycobacterial chemotherapy.

*Patient 3.* The patient became spontaneously positive to the tuberculin purified protein derivative (PPD) skin test at age 11 months. There was no family history of tuberculosis. A chest radiograph showed no abnormal lesion. The PPD skin test became negative after 6 months of prophylactic treatment with isoniazid, and he was subsequently inoculated with BCG. Nine months later, he presented with claudication and limitation in rotation and anteflexion of the neck. Radiographic studies showed multiple destructive lesions over eight bones. Cultures from bone biopsy specimens grew *M. bovis*. He was successfully treated with isoniazid, rifampicin, and streptomycin.

*Patient 4.* The patient presented with fever, claudication, and knee swelling 1 year after BCG vaccination. He had osteomyelitis in the distal metaphysis of the right femur. Cultures from bone curettage specimens grew *M. bovis*. The lesion resolved with isoniazid, rifampicin, and ethambutol treatment.

*Patient 5.* The patient presented with claudication and knee swelling 18 months after BCG vaccination. Radiographic studies revealed lytic lesions in the left femur and tibia. Open biopsy was performed, but no organisms were isolated. The lesion improved gradually with antibiotics. Nine months after initial presentation, he was evaluated again with the same lesion. Cultures from a bone curettage specimen grew *M. bovis*. The lesion resolved with isoniazid, rifampicin, and ethambutol therapy.

*Patient 6.* The patient presented with a limp, wryneck, and submandibular swelling 5 months after BCG vaccination. Radiographic studies showed multiple osteolytic lesions over 4 bones. He was treated under the tentative diagnosis of Langerhans cell histiocytosis for 8 months without improvement. Sixteen months after vaccination, additional osteolytic lesions appeared in several bones and skin lesions, with red papules scattered over the whole body. Cultures from bone and skin biopsy specimens grew *M. bovis*. He was successfully treated with isoniazid, rifampicin, and streptomycin.

None of the children had histories of increased susceptibility to other bacterial or viral infections. Responses to phytohemagglutinin were examined in patients 1, 4, and 6, but no abnormalities were found.

### DNA Extraction

Genomic DNA was obtained from peripheral blood mononuclear cells (PBMC) with the QIAamp DNA extraction kit (Qiagen).

### cDNA Preparation

Total RNA was isolated from PBMC by use of ISOGEN reagent (Nippon Gene). cDNA was synthesized by using a first-strand cDNA synthesis kit (Amersham Pharmacia Biotech) with random hexamers.

### In Vitro Cytokine Production by PBMC

PBMC were stimulated by use of OK432 (a heat- and penicillin-treated lyophilized powder of *Streptococcus pyogenes* strain Su, 10 mg/mL; Chugai) or BCG (10 mg/mL, BCG Tokyo 172; Japan BCG Laboratory) for 24 h (IL-12) or 72 h (IFN-γ). For the IL-12–dependent IFN-γ assay, PBMC were stimulated with recombinant (r) IL-12 (40 ng/mL; R&D Systems) in the presence or absence of rIL-18 (100 ng/mL; R&D Systems) for 72 h. Supernatants were assayed for IL-12 and IFN-γ with IL-12 (R&D Systems) and IFN-γ (PharMingen) sandwich ELISA kits, according to the manufacturer's instructions.

### cDNA Sequence Analysis

To analyze mutations for the coding regions of *IFNGR1*, *IFN-GR2*, *IFNG*, *IL12B*, *IL12RB1*, and *STAT-1*, cDNA sequences were determined by polymerase chain reaction (PCR) by using primer pairs and subsequent direct sequencing. For *IFNGR1*, we used 5′-GTGACGGAAGTGACGTAAGG-3′ and 5′-CGGCATACAG-CAAATTCTTC-3′, 5′-TCTGATCATGTTGGTGATCCA-3′ and 5′-CAGATGAATACCAGGCTAAGCA-3′, 5′ TGTGTGGGGTG-

TTACAACTGAA-3′ and 5′-GATGCTGCCAGGTTCAGACT-3′, and 5′-ACCGAAGACAATCCAGGAAAAG-3′ and 5′-CAGACTTCAAAGTTGGTGCAA-3. For *IFNGR2*, we used 5′-TGCTGCTGCTCGGAGTCTT-3′ and 5′-GCCTTTGACCTGTTGGATTC-3′ and 5′-GGAGAAGGCTCCCTCATCAT-3′ and 5′-AACTCTAGCAGCTCCGATGG-3′. For *IFNG*, we used 5′-GCTTGATACAAGAACTACTG-3′ and 5′-CAGTCACAGGATATAGGAAT-3′. For *IL12B*, we used 5′-TTTCAGGGCCATTGGACTC-3′ and 5′-TGTAGCAGCTCCGCACGT-3′ and 5′-CATTCAGTGTCAAAAGCAG-3′ and 5′-GTCTATTCCGTTGTGTCTT-3′. For *IL12RB1*, we used 5′-AACCTCGCAGGTGGCAGAGA-3′ and 5′-TCCGCAGTCGCCCAACTT-3′, 5′-TTGGTGCTGAGGTGCAGTTC-3′ and 5′-GTCATGCTCTGAGCCCGG-3′, 5′-GCTCTGAATATCAGCGTCGGAA-3′ and 5′-CAGAAACCTGCACTTCGATGCT-3′, and 5′-GGTGTAGCCTACACGGTGC-3′ and 5′-GGGCGAGTCACTCACCCT-3′. For *STAT-1*, we used 5′-GCTGTCTAGGTTAACGTTCGCA-3′ and 5′-TATTCCCCGACTGAGCCTGAT-3′, 5′-AAATTCTGGAAAACGCCCAGAG-3′ and 5′-GAAAAGACTGAAGGTGCGGTC-3′, 5′-GCCCAATGCTTGCTTGGAT-3′ and 5′-AGGTCAATTACCAAACCAGGCT-3′, 5′-GGGCACGCACACAAAAGT-3′ and 5′-TCTCGCTCCTTGCTGATGAAG-3′, 5′-TCCCTTCTGGCTTTGGATTG-3′ and 5′-TCGTCAAACTCCTCAGGAGACA-3′, and 5′-TTCCATGCGGTTGAACCCT-3′ and 5′-AGATGCATGATGCCCTTCAGAG-3′.

PCR products were purified and analyzed by direct sequencing by using a fluorescent dideoxy-terminator method and an ABI 310 DNA sequencer (Perkin-Elmer). Detected mutations of *IFNGR1* (818del4 and 811del4) were confirmed by PCR with genomic DNA by using primers 5′-TCTTAACTCTGCCTATTCAC-3′ and 5′-GGACTTGGGTAATATTATGC-3′ designed within exon 6, followed by direct sequencing.

### Flow Cytometry

Two-color flow cytometric analysis was performed with EPICS XL (Beckman Coulter), as follows: PBMC were stained with mouse anti–IFN-γ receptor 1 (IFN-γR1) monoclonal antibody (MAb; Genzyme), followed by rat phycoerythrin anti-mouse immunoglobulin antibody (Becton Dickinson). Cells were washed twice and stained with phycoerythrin 5.1 (PC5)–anti-CD14 MAb (Coulter Immunotech). Analysis of IFN-γR1 expression was performed on cells within the gate set for monocytes, by use of PC5 and side scatters.

## Results

*In vitro cytokine production by PBMC.* PBMC from all patients and from healthy control subjects produced appreciable amounts of IFN-γ by stimulation with OK423, BCG, or rIL-12 in the presence or absence of rIL-18. In addition, production of IL-12 protein in the supernatants from PBMC stimulated with OK432 or BCG was observed in all patients and in healthy control subjects (data not shown).

*cDNA sequence analysis.* Sequence analysis of the coding region of *IFNGR1* revealed heterozygous small deletions in 3 of the 6 patients. Patient 1 had a 4-nt deletion, either AAGA at nt 811, AGAA at nt 812, or GAAA at nt 813 (designated "811del4"), and patients 2 and 3 had another 4-nt deletion, either AATT at nt 816, ATTA at nt 817, TTAA at nt 818, or TAAT at nt 819 (designated "818del4"), in exon 6 of the *IFNGR1* open-reading frame. The same mutation found in patient 2 was also found in his father (patient 2′). None of the remaining 3 patients or the 9 unaffected family members of patients 1–3 had *IFNGR1* mutations (figure 1). The nucleotide deletions in exon 6, which were found in 3 patients and in 1 of the fathers, created a premature stop codon at the same position (nt 827–829), downstream of the segment encoding the transmembrane domain. These mutations were confirmed by PCR with genome DNA. Sequence analysis of the coding regions of *IFNGR2*, *IFNG*, *IL12B*, *IL12RB1*, and *STAT-1* revealed no defects or abnormalities in 3 patients without *IFNGR1* mutations.

*Flow cytometry.* The IFN-γR1 expression levels on monocytes in patients 1–3 were significantly higher than in adult control subjects. However, patients 4–6 had normal receptor expression when compared with control samples (data not shown).

## Discussion

In this study, we screened 6 Japanese children with BCG osteomyelitis for defects of IL-12–dependent, IFN-γ–mediated

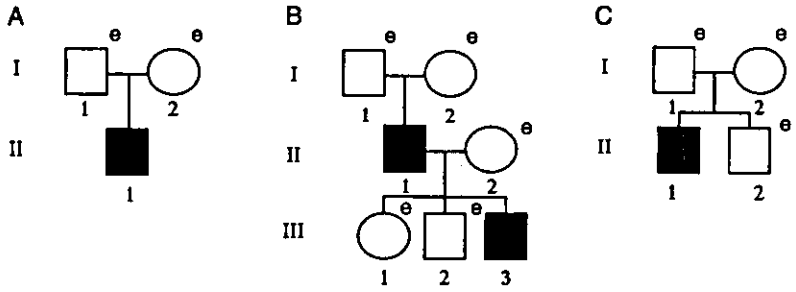


**Figure 1.** Pedigrees of 3 families with partial dominant interferon-γ receptor 1 deficiency. Each kindred is designated by a capital letter (A–C), each generation by a Roman number (I–III), and each individual by an Arabic number (1–3). Patients with mutations in *IFNGR1* are shown as filled squares. e, Examined.

immunity and identified heterozygous small deletions in exon 6 of *IFNGR1* in 3 patients and in 1 of their fathers. One was a known deletion, 818del4, and the other was novel, 811del4. These mutations were consistent with those observed in partial dominant IFN-γR1 deficiency, which was first reported by Jouanguy et al. [4]. Mutant proteins are expressed on the cell surface and normally bind IFN-γ but cannot transduce signal because of a lack of JAK1 and STAT-1 binding sites [4]. As observed in our patients, absence of the IFN-γR1 recycling motif causes increased expression of the receptor, which leads to dominant negative effects. Residual IFN-γ responsiveness is thought to be mediated from the normal allele in these heterozygous persons [4]. In the present study, only 1 kindred manifested autosomal dominant inheritance, and others occurred sporadically. A possible underlying mechanism of these small deletion hot spots might be explained as follows: The sequences surrounding nt 818 may serve as templates for slipped mispairing during DNA replication or as putative arrest sites for polymerase α at the replication fork [4].

The severity of the clinical features of patients with partial dominant IFN-γR1 deficiency has been reported to be intermediate between those of the complete and partial recessive deficiencies [4]. Of note, even the poorly virulent BCG Tokyo 172 strain can be harmful in partially dominant IFN-γR1–deficient patients. The 4 patients in the present study responded well to antimycobacterial therapy and had relatively good clinical outcome. Even so, early genetic diagnosis of this disorder would be beneficial because BCG vaccination is avoidable and optimal antimycobacterial treatment is applicable in cases of mycobacterial infection.

Inheritable disorders of IL-12–dependent, IFN-γ–mediated immunity apparently are not confined to any ethnic group or geographic region. As for partial dominant IFN-γR1 deficiency, few patients of Asian origin have been reported. Our study found this disorder was predominant in Japanese patients who developed BCG osteomyelitis. Although BCG osteomyelitis is one characteristic feature of partial dominant IFN-γR1 deficiency, we could not detect any mutations of this gene in the other 3 patients. Moreover, we detected no mutations in the coding regions of *IFNGR2, IL12B, IL12RB1,* or *STAT-1.* These patients presented with relatively milder clinical symptoms, compared with persons with partial dominant IFN-γR1 deficiency: 2 had solitary lesions, and all 3 had single episodes. In children with IFN-γR1 deficiency, all 3 had multiple lesions and 2 had recurrence. There were no obvious defects, by conventional laboratory examinations, in in vitro IL-12/IFN-γ production or T cell function in both *IFNGR1*-intact and *IFNGR1*-deficient patients, which made differentiation difficult without flow cytometry and sequence analyses. It remains possible that these children might have an abnormality in different genes involved in IL-12–dependent, IFN-γ–mediated immunity or in other antimicrobial pathways mediated by cytolytic T cells, such as inducible nitric oxide synthase [14] and granulysin [15].

In conclusion, we identified partial *IFNGR1* mutations, 818del4 and the novel deletion 811del4, in 3 Japanese children with BCG osteomyelitis who had recurrent and disseminated mycobacterial infections and in 1 of their fathers. Further investigation is needed to reveal unknown defects in IFN-γ–mediated immunity associated with predisposition to mycobacterial infections.

**Acknowledgment**

We thank Yasushi Takahata for technical assistance.

**References**

1. Lotte WHO, Poisson N, Engbaek H, et al. Second IUATLD study on complications induced by intradermal BCG-vaccination. Bull Int Union Tuberc Lung Dis **1988**;63:47–59.
2. Newport MJ, Huxley CM, Huston S, et al. A mutation in the interferon-γ receptor gene and susceptibility to mycobacterial infection. N Engl J Med **1996**;335:1941–9.
3. Jouanguy E, Altare F, Lamhamedi S, et al. Interferon-γ-receptor deficiency in an infant with fatal bacille Calmette-Guérin infection. N Engl J Med **1996**;335:1956–61.
4. Jouanguy E, Lamhamedi-Cherradi S, Lammas D, et al. A human IFNGR1 small deletion hotspot associated with dominant susceptibility to mycobacterial infection. Nat Genet **1999**;21:370–8.
5. Dorman SE, Holland SM. Mutation in the signal-transducing chain of the interferon γ receptor and susceptibility to mycobacterial infection. J Clin Invest **1998**;101:2364–9.
6. Doffinger R, Jouanguy E, Dupuis S, et al. Partial interferon-γ receptor signaling chain deficiency in a patient with bacille Calmette-Guérin and *Mycobacterium abscessus* infection. J Infect Dis **2000**;181:379–84.
7. Altare F, Lammas D, Revy P, et al. Inherited interleukin 12 deficiency in a child with bacille Calmette-Guérin and *Salmonella enteritidis* disseminated infection. J Clin Invest **1998**;102:2035–40.
8. Altare F, Ensser A, Breiman A, et al. Interleukin-12 receptor β1 deficiency in a patient with abdominal tuberculosis. J Infect Dis **2001**;184:231–6.
9. Sakai T, Matsuoka M, Aoki M, Nosaka K, Mitsuya H. Missense mutation of the interleukin-12 receptor β1 chain–encoding gene is associated with impaired immunity against *Mycobacterium avium* complex infection. Blood **2001**;97:2688–94.
10. Aksu G, Tirpan C, Cavusoglu C, et al. *Mycobacterium fortuitum-chelonae* complex infection in a child with complete interleukin-12 receptor β1 deficiency. Pediatr Infect Dis J **2001**;20:551–3.
11. Dupuis S, Dargemont C, Fieschi C, et al. Impairment of mycobacterial but not viral immunity by a germline human STAT1 mutation. Science **2001**;293:300–3.
12. Roesler J, Kofink B, Wendisch J, et al. *Listeria monocytogenes* and recurrent mycobacterial infections in a child with complete interferon-γ-receptor (IFNγR1) deficiency: mutational analysis and evaluation of therapeutic options. Exp Hematol **1999**;27:1368–74.
13. Dorman SE, Uzel G, Roesler J, et al. Viral infections in interferon-γ receptor deficiency. J Pediatr **1999**;135:640–3.
14. Garcia I, Guler R, Vesin D, et al. Lethal *Mycobacterium bovis* bacillus Calmette-Guérin infection in nitric oxide synthase 2–deficient mice: cell-mediated immunity requires nitric oxide synthase 2. Lab Invest **2000**;80:1385–97.
15. Stenger S, Hanson DA, Teitelbaum R, et al. An antimicrobial activity of cytolytic T cells mediated by granulysin. Science **1998**;282:121–5.

that the biophysical underpinning of such a nonlinear operation can be described mechanistically in a single neuron. □

## Methods

### Electrophysiology

Dissections and extracellular recordings from 45 descending contralateral movement detector (DCMD) neurons were as described in refs 12 and 20. We used extra-cellular recordings from the DCMD to monitor the spike activity of the LGMD because their spiking outputs match perfectly (Fig. 4a). Intracellular recordings from the LGMD ($n = 91$ animals) were obtained using glass microelectrodes filled with 2 M potassium acetate solution (30–80 MΩ). Typical intracellular recordings times were 40 min – 1 h. Stainings (Fig. 1a) were obtained by iontophoresis of Lucifer yellow (2% in aqueous solution). Local drug injections were performed using pulled and microforged glass micropipettes (final diameter, ~1 μm), backfilled with PCTX (5 mM) or TTX (1 μM) in aqueous solution and 0.5% (w/v) Fast green for visualization. Further technical details are available in Supplementary Information. Intracellular signals were amplified in bridge or DCC mode using an Axoclamp 2B (Axon Instruments) or SEL-10 (NPI) amplifier.

### Visual stimulation

Visual stimulation procedures have been described previously[12,20]. Briefly, black squares approaching perpendicular to the main body axis towards the eye (duration, 0.6–5.7 s) at various values of $l/|v|$ were presented in pseudo random order. Background flow stimuli consisted of alternating bright and grey (30% contrast) concentric rectangles moving outwards towards the screen boundaries at constant temporal frequency. For the slow-flow stimulus (Fig. 2a), the temporal frequency of light/dark transitions was set between 6 and 12 Hz. For the fast stimulus (Figs 2c, 3a, b, d), the temporal frequency was 50 Hz. Further details as well as procedures used to minimize habituation[29] of the responses are described in Supplementary information.

### Data analysis

Data collection was performed using a PCI data acquisition card (UEI) and custom software[20]. Sample rates were 10 kHz for extracellular, and 20 kHz for intracellular, recordings. Data analysis methods followed refs 12 and 20. Median filtering and fits of the LGMD/DCMD firing rate, $f(t)$, with various models are described in Supplementary Information. The relation between average membrane potential, $\langle \bar{V}_m \rangle$, and firing rate, $\langle f \rangle$, (Fig. 4d) was obtained by averaging across trials membrane potential and instantaneous firing rate over 5-ms time windows and plotting one variable against the other. Linear ($\langle f \rangle = \alpha \langle \bar{V}_m \rangle$), power law ($\langle f \rangle = \alpha \langle \bar{V}_m \rangle^n$) and exponential ($\langle f \rangle = \exp(\alpha \langle \bar{V}_m \rangle) - 1$) models depicted in Fig. 4d were fitted using maximum likelihood. Statistical tests followed ref. 30.

Received 1 August; accepted 20 September 2002; doi:10.1038/nature01190.


1. Reichardt, W. Autokorrelations-Auswertung als Funktionsprinzip des Zentralnervensystems. *Z. Naturforsch.* **12**, 448–457 (1957).
2. Barlow, H. B. & Levick, W. R. The mechanisms of directionally selective units in rabbit's retina. *J. Physiol. (Lond.)* **178**, 477–504 (1965).
3. McAdams, C. J. & Maunsell, J. H. R. Effects of attention on orientation-tuning functions of single neurons in macaque cortical area V4. *J. Neurosci.* **19**, 431–441 (1999).
4. Sun, H. & Frost, B. J. Computation of different optical variables of looming objects in pigeon nucleus rotundus neurons. *Nature Neurosci.* **1**, 296–303 (1998).
5. Pena, J. L. & Konishi, M. Auditory spatial receptive fields created by multiplication. *Science* **292**, 249–252 (2001).
6. Torre, V. & Poggio, T. A synaptic mechanism possibly underlying directional selectivity to motion. *Proc. R. Soc. Lond. B* **202**, 409–416 (1978).
7. Andersen, R. A., Essick, G. K. & Siegel, R. M. Encoding of spatial location by posterior parietal neurons. *Science* **23**, 456–458 (1985).
8. Yuste, R. & Tank, D. Dendritic integration in mammalian neurons, a century after Cajal. *Neuron* **16**, 701–716 (1996).
9. Koch, C. *Biophysics of Computation: Information Processing in Single Neurons* (Oxford Univ. Press, Oxford, 1998).
10. Chance, F. S., Abbott, L. F. & Reyes, A. D. Gain modulation from background synaptic input. *Neuron* **35**, 773–782 (2002).
11. Hatsopoulos, N., Gabbiani, F. & Laurent, G. Elementary computation of object approach by a wide-field visual neuron. *Science* **270**, 1000–1003 (1995).
12. Gabbiani, F., Krapp, H. G. & Laurent, G. Computation of object approach by a wide-field, motion-sensitive neuron. *J. Neurosci.* **19**, 1122–1141 (1999).
13. Rind, F. C. & Bramwell, D. I. Neural network based on the input organization of an identified neuron signaling impending collision. *J. Neurophysiol.* **75**, 967–985 (1996).
14. Rind, F. C. Intracellular characterization of neurons in the locust brain signaling impending collision. *J. Neurophysiol.* **75**, 986–995 (1996).
15. Wagner, H. Flow field variables trigger landing in flies. *Nature* **297**, 147–148 (1982).
16. Wicklein, M. & Strausfeld, N. J. Organization and significance of neurons that detect change of visual depth in the hawk moth *Manduca sexta*. *J. Comp. Neurol.* **424**, 356–376 (2000).
17. Schlotterer, G. R. Response of the locust descending movement detector neuron to rapidly approaching and withdrawing visual stimuli. *Can. J. Zool.* **55**, 1372–1376 (1977).
18. Rind, F. C. & Simmons, P. J. Orthopteran DCMD neuron: a reevaluation of responses to moving objects. I. Selective responses to approaching objects. *J. Neurophysiol.* **68**, 1654–1666 (1992).
19. Robertson, R. M. & Johnson, A. G. Retinal image size triggers obstacle avoidance in flying locusts. *Naturwissenschaften* **80**, 176–178 (1993).
20. Gabbiani, F., Mo, C. & Laurent, G. Invariance of angular threshold computation in a wide-field looming-sensitive neuron. *J. Neurosci.* **21**, 314–329 (2001).
21. O'Shea, M. & Rowell, C. H. F. Protection from habituation by lateral inhibition. *Nature* **254**, 53–55 (1975).
22. Rowell, C. H. F., O'Shea, M. & Williams, J. L. D. The neuronal basis of a sensory analyser, the acridid movement detector system. IV. The preference for small field stimuli. *J. Exp. Biol.* **68**, 157–185 (1977).
23. Rind, F. C. & Simmons, P. J. Local circuits for the computation of object approach by an identified visual neuron in the locust. *J. Comp. Neurol.* **395**, 405–415 (1998).
24. Rauh, J. J., Lummis, S. C. R. & Sattelle, D. B. Pharmacological and biochemical properties of insect GABA receptors. *Trends Pharmacol.* **11**, 325–329 (1990).
25. Warzecha, A. K., Egelhaaf, M. & Borst, A. Neural circuit tuning fly visual interneurons to motion of small objects. 1. Dissection of the circuit by pharmacological and photoinactivation techniques. *J. Neurophysiol.* **69**, 329–339 (1993).
26. Zanker, J. M., Srinivasan, M. V. & Egelhaaf, M. Speed tuning in elementary motion detectors of the correlation type. *Biol. Cybern.* **80**, 109–116 (1999).
27. Mead, C. *Analog VLSI and Neural Systems* (Addison-Wesley, Boston, 1989).
28. Koch, C., Bernander, O. & Douglas, R. J. Do neurons have a voltage or a current threshold for action potential initiation? *J. Comput. Neurosci.* **2**, 63–82 (1995).
29. Rowell, C. H. F. in *Experimental Analysis of Insect Behavior* (ed. Browne, L. B.) 87–99 (Springer, New York, 1974).
30. Galant, A. R. *Non-linear Statistical Models* (Wiley & Sons, New York, 1987).


**Supplementary Information** accompanies the paper on *Nature*'s website (http://www.nature.com/nature).

**Acknowledgements** We thank C. Mo for technical assistance with the experiments presented in Fig. 2, S. Potter for help with two-photon confocal microscopy, and J. Maunsell for comments. This work was supported by the Sloan Foundation, the National Institute of Mental Health (F.G., C.K.), the National Institute for Deafness and Communication Disorders (G.L.), the McKnight Foundation (G.L.) and the Center for Neuromorphic Engineering as part of the NSF Engineering Research Center programme. H.G.K. was supported by a travel grant of the Deutsche Forschungsgemeinschaft. F.G. is an Alfred P. Sloan research fellow.

**Competing interests statement** The authors declare that they have no competing financial interests.

**Correspondence** and requests for materials should be addressed to F.G. (e-mail: gabbiani@bcm.tmc.edu).

# Essential role for TIRAP in activation of the signalling cascade shared by TLR2 and TLR4

**Masahiro Yamamoto*†, Shintaro Sato*†, Hiroaki Hemmi*†, Hideki Sanjo*†, Satoshi Uematsu*†, Tsuneyasu Kaisho*†‡, Katsuaki Hoshino*†, Osamu Takeuchi*†, Masaya Kobayashi*†, Takashi Fujita§, Kiyoshi Takeda*† & Shizuo Akira*†**

** Department of Host Defense, Research Institute for Microbial Diseases, Osaka University, and † Solution Oriented Research for Science and Technology, Japan Science and Technology Corporation, 3-1 Yamada-oka, Suita, Osaka 565-0871, Japan*

*‡ RIKEN Research Center for Allergy and Immunology, 1-7-22 Suehiro-cho, Tsurumi-ku, Yokohama, Kanagawa 230-0045, Japan*

*§ Department of Tumor Cell Biology, The Tokyo Metropolitan Institute of Medical Science, 3-18-22 Honkomagome, Bunkyo-ku, Tokyo 113-8613, Japan*

Signal transduction through Toll-like receptors (TLRs) originates from their intracellular Toll/interleukin-1 receptor (TIR) domain, which binds to MyD88, a common adaptor protein containing a TIR domain[1–4]. Although cytokine production is completely abolished in MyD88-deficient mice, some responses to lipopolysaccharide (LPS), including the induction of interferon-inducible genes and the maturation of dendritic cells, are still observed[5–7]. Another adaptor, TIRAP (also known as Mal), has been cloned as a molecule that specifically associates with TLR4 and thus may be responsible for the MyD88-independent response[8,9]. Here we report that LPS-induced splenocyte proliferation and cytokine production are abolished in mice lacking TIRAP. As in MyD88-deficient mice, LPS activation of the nuclear factor NF-κB and mitogen-activated protein kinases

  

**is induced with delayed kinetics in TIRAP-deficient mice[5]. Expression of interferon-inducible genes and the maturation of dendritic cells is observed in these mice; they also show defective response to TLR2 ligands, but not to stimuli that activate TLR3, TLR7 or TLR9. In contrast to previous suggestions, our results show that TIRAP is not specific to TLR4 signalling and does not participate in the MyD88-independent pathway. Instead, TIRAP has a crucial role in the MyD88-dependent signalling pathway shared by TLR2 and TLR4.**

To examine the physiological role of TIRAP, we generated TIRAP-deficient mice by gene targeting. A targeting vector was constructed in which the two exons encoding the TIR domain were replaced with the neomycin resistance (*neo*$^R$) gene (Fig. 1a). Homologous recombination in embryonic stem (ES) cells was confirmed by Southern blot analysis, and correctly targeted ES cells were used to generate mice with the mutated allele (Fig. 1b). Expression of TIRAP mRNA in the mutant mice was examined by northern blot analysis. When we used the amino-terminal fragment of TIRAP cDNA as a probe, we detected transcripts from the mutant mice with almost the same size as those of wild-type mice (Fig. 1c). Polymerase chain reaction with reverse transcription analysis (RT–PCR) showed, however, that the *neo*$^R$ gene was inserted into the mouse *Tirap* gene in the mutant mice, leading to a stop codon in the N-terminal portion of TIRAP (Supplementary Fig. 1). Immunoblot analysis of splenocytes confirmed that disruption of the *Tirap* gene abolished the expression of TIRAP protein (Fig. 1d). TIRAP-deficient mice were healthy and had a normal composition of B and T lymphocytes, as determined by flow cytometry (data not shown).

Because TIRAP was identified as an adaptor that specifically associates with TLR4, we first analysed the response to LPS in TIRAP-deficient mice[8,9]. Stimulation with LPS induced dose-dependent proliferation and augmented the expression of major histocompatibility complex (MHC) class II molecules in wild-type splenocytes, whereas proliferation and augmentation of MHC class II expression was severely impaired in TIRAP-deficient splenocytes (Fig. 2a and b). Although TLR and the interleukin-1 (IL-1) receptor family share some signalling molecules, such as MyD88, both wild-type and TIRAP-deficient splenocytes proliferated to the same extent in response to IL-1 plus PHA, showing that TIRAP-deficient splenocytes are not defective in IL-1-induced proliferation (ref. 10 and Fig. 2c).

We analysed the LPS-induced production of inflammatory cytokines from peritoneal macrophages. Wild-type macrophages produced IL-6, tumour-necrosis factor-α (TNF-α) and IL-12 in response to LPS (Fig. 3a, b); however, LPS did not stimulate the production of IL-6, TNF-α or IL-12 in TIRAP-deficient macrophages. Wild-type mice showed an increased serum concentration of IL-6 after a high dose injection of LPS and died within 96 h (Fig. 3c and d). By contrast, TIRAP-deficient mice were completely resistant to LPS-induced shock and produced only a small amount of IL-6.

Wild-type and TIRAP-deficient macrophages produced similar amounts of IL-6, TNF-α and IL-12 in response to CpG DNA, a TLR9 ligand, and the synthetic compound R-848, a TLR7 ligand

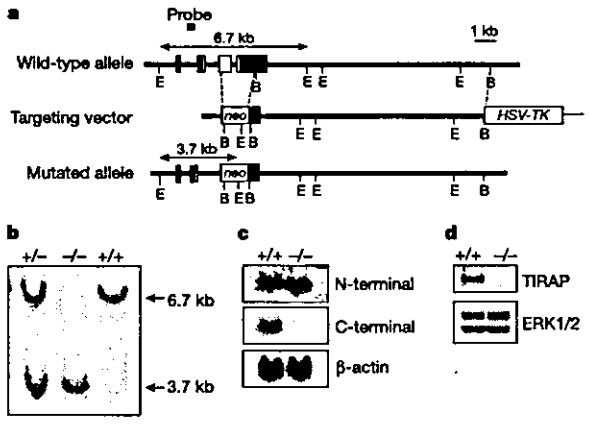


**Figure 1** Targeted disruption of the murine *Tirap* gene. **a**, Structure of the mouse *Tirap* gene, the targeting vector and the predicted disrupted gene. Open boxes denote the coding exon. E, *Eco*RI; B, *Bam*HI. **b**, Southern blot analysis of offspring from the heterozygote intercrosses. Genomic DNA was extracted from mouse tails, digested with *Eco*RI, separated by electrophoresis and hybridized with the radiolabelled probe indicated in **a**. Southern blotting gave a single 6.7-kb band for wild-type (+/+), a 3.7-kb band for homozygous (−/−) and both bands for heterozygous (+/−) mice. **c**, Northern blot analysis of embryonic fibroblasts. Total RNA (10 μg) extracted from embryonic fibroblasts was separated by electrophoresis, transferred to nylon membrane and hybridized using the TIRAP N-terminal or C-terminal fragment as a probe. The same membrane was rehybridized with a β-actin probe. **d**, Western blot analysis of splenocytes. The cell lysates were immunoprecipitated and immunoblotted with a polyclonal antibody against TIRAP. The same lysates were also blotted with antibodies against ERK1 and ERK2 to monitor protein expression.

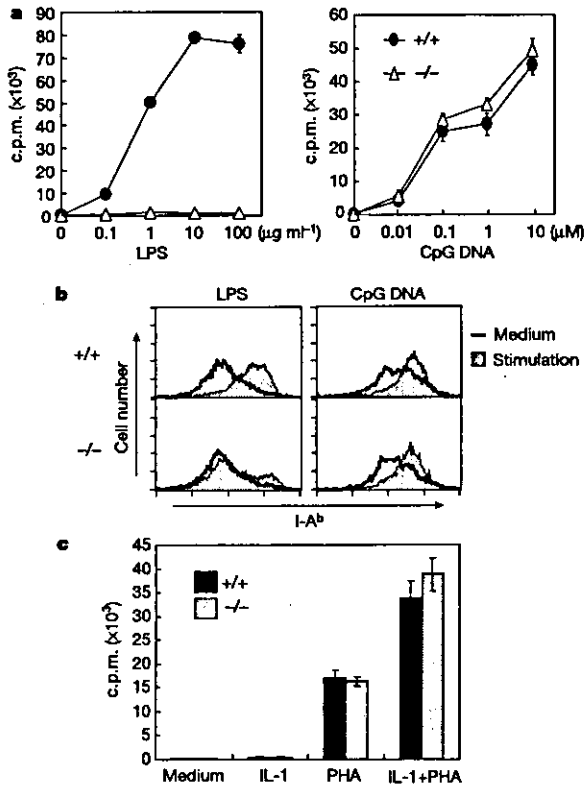


**Figure 2** Impaired response to LPS in TIRAP-deficient splenocytes. **a**, Proliferation of splenocytes stimulated by LPS and CpG DNA. Wild-type (+/+) and TIRAP-deficient (−/−) splenocytes were cultured with the indicated concentration of LPS or CpG DNA for 48 h. [$^3$H]thymidine (1 μCi) was pulsed for the last 12 h, and [$^3$H]thymidine incorporation was measured by liquid scintillation counting. **b**, Splenic B cells were cultured with 1 μg ml$^{-1}$ LPS or 0.1 μM CpG DNA. After 48 h, cells were collected, stained with a biotinylated antibody against I-A$^b$ followed by streptavidin–PE, and analysed by FACS. **c**, Splenocytes from wild-type and TIRAP-deficient mice were incubated with 10 ng ml$^{-1}$ IL-1β in the presence of 10 ng ml$^{-1}$ PHA for 72 h. [$^3$H]thymidine was pulsed for the last 12 h, and uptake of [$^3$H] was measured.

(refs 11, 12, and Fig. 3a). Stimulation of macrophages with poly(I:C), a TLR3 ligand, induced the mRNA expression of interferon-β (IFN-β), as well as IL-6 and TNF-α, in both wild-type and TIRAP-deficient mice (ref. 13 and Fig. 3e).

We also analysed the production of inflammatory cytokines in response to the mycoplasma-derived lipopeptide MALP-2, and to *Staphylococcus aureus* peptidoglycan (PGN), which are both TLR2 ligands (refs 14, 15, and Fig. 3f). Wild-type macrophages showed dose-dependent production of IL-6, TNF-α and IL-12 in response to MALP-2 and PGN. In contrast, the MALP-2- or PGN-induced production of these cytokines was severely impaired in TIRAP-deficient mice. Together, these results show that TIRAP-deficient mice have an impaired response to TLR2 and TLR4 ligands, but a normal response to microbial components recognized by TLR3, TLR7 and TLR9.

Next, we analysed the activation of intracellular signalling cascades in response to LPS, MALP-2 and R-848. In wild-type macrophages, stimulation with LPS resulted in enhanced DNA-binding activity of NF-κB (Fig. 4a, left). In TIRAP-deficient and MyD88-deficient macrophages, this NF-κB DNA-binding activity was not induced at 10 min but was significantly induced at 20 min. Stimulation with LPS induced the activation of mitogen-activated protein (MAP) kinases, including extracellular-signal-regulated kinases (ERK) 1 and 2, p38 and Jun N-terminal kinase (JNK), in wild-type macrophages (Fig. 4b, left). In TIRAP-deficient macrophages, however, the LPS-induced activation of these kinases was detected with delayed kinetics. Thus, the LPS-induced activation of signalling molecules is compromised in TIRAP-deficient mice, whose phenotype is similar to that of MyD88-deficient mice[5].

MALP-2 induced NF-κB DNA binding activity in macrophages. However, NF-κB activation was severely impaired in TIRAP-deficient mice (Fig. 4a, middle). In addition, the MALP-2-induced activation of ERK1/ ERK2, p38 and JNK was not observed in TIRAP-deficient macrophages (Fig. 4b, middle). By contrast, the

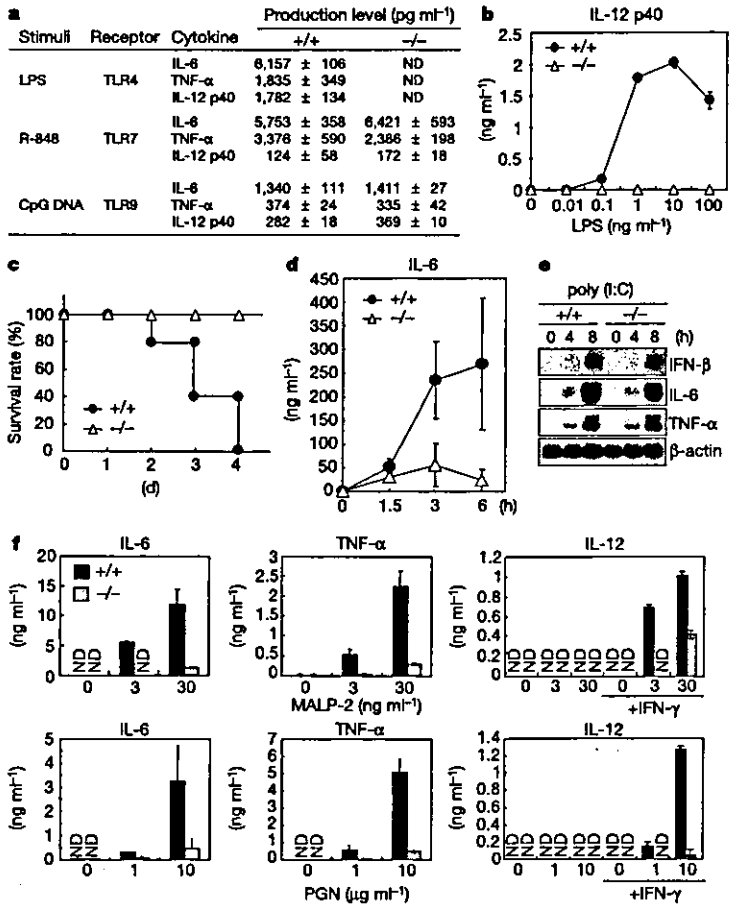


**Figure 3** Cytokine production in peritoneal macrophages in response to TLR ligands. **a**, Peritoneal macrophages from wild-type (+/+) and TIRAP-deficient (−/−) mice were cultured with 1 ng ml$^{-1}$ LPS, 10 nM R-848 or 1 μM CpG DNA in the presence (IL-12) or absence (IL-6 and TNF-α) of 30 ng ml$^{-1}$ IFN-γ for 24 h. Concentrations of IL-6, TNF-α and IL-12 in the culture supernatants were measured by enzyme-linked immunoabsorbent assay (ELISA). Data are the means ± s.d. of triplicates. ND, not detected. **b**, Peritoneal macrophages were stimulated with the indicated concentrations of LPS in the presence of 30 ng ml$^{-1}$ IFN-γ for 24 h, and the supernatants were analysed for IL-12 by ELISA. Data are the means ± s.d. of triplicates. **c**, Age-matched wild-type ($n = 5$) and TIRAP-deficient ($n = 5$) mice were injected intraperitoneally with 2.0 mg of LPS (*Escherichia coli* 055:B5). Mortality was assessed daily for 4 d. **d**, TIRAP-deficient and wild-type mice were intraperitoneally injected with 1.5 mg of LPS (*E. coli* 055:B5). Sera were taken after the indicated period of time, and serum concentrations of IL-6 were determined by ELISA. Data are the means ± s.d. of samples from three mice. **e**, Peritoneal macrophages were stimulated with 50 μg ml$^{-1}$ poly (I:C) for 4 and 8 h. Total RNA was extracted and analysed for expression of IFN-β, IL-6 and TNF-α mRNA by northern blotting. **f**, Peritoneal macrophages were stimulated with the indicated concentrations of MALP-2 or PGN for 24 h. Production of IL-6, TNF-α and IL-12 in the culture supernatants was measured by ELISA. Data are the means ± s.d. of triplicates. ND, not detected.

R-848-induced activation of NF-κB and MAP kinases was not altered in TIRAP-deficient macrophages (Fig. 4a and b, right). We also analysed activity of IRAK-1 by *in vitro* kinase assay (Fig. 4c). In wild-type macrophages, stimulation with LPS, MALP-2 and R-848 induced autophosphorylation of IRAK-1. In TIRAP-deficient mice, however, IRAK-1 was not activated in response to either LPS or MALP-2, but was activated normally in response to R-848. Thus, similar to MyD88, TIRAP acts at the level of IRAK-1 signalling; however, unlike activation mediated by MyD88, the TIRAP-mediated activation of IRAK-1 is specific to TLR2 and TLR4.

The TLR4 signal consists of the MyD88-dependent and -independent pathways[1,5–7]. The MyD88-independent pathway contributes to the LPS-induced expression of IFN-inducible genes and the maturation of dendritic cells[6,7]. *In vitro* studies have indicated that

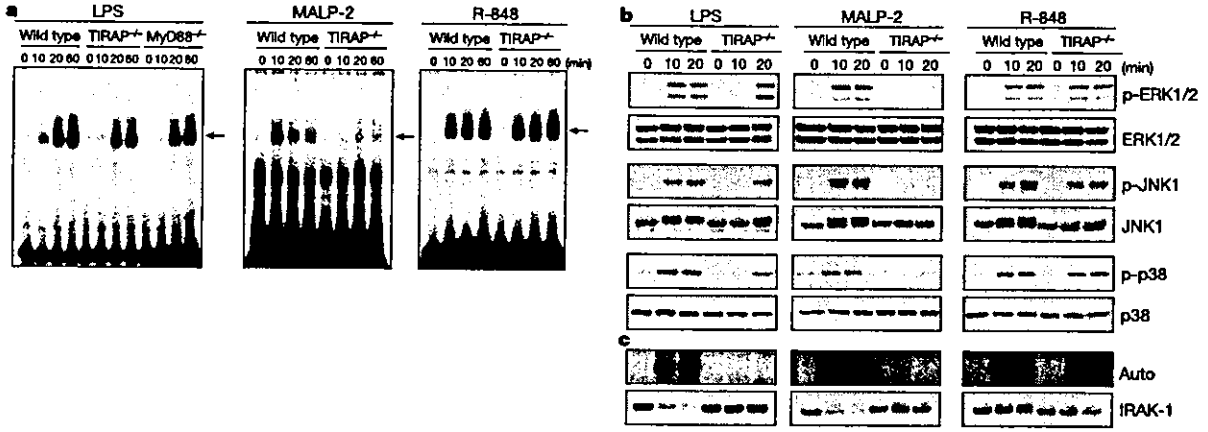


**Figure 4** Activation of signalling cascades in response to TLR2, TLR4 and TLR7 ligands in peritoneal macrophages. **a**, Peritoneal macrophages were stimulated with 100 ng ml$^{-1}$ LPS (left), 3 ng ml$^{-1}$ MALP-2 (middle) or 10 nM R-848 (right) for the indicated durations. Nuclear extracts were prepared and NF-κB DNA-binding activity was determined by electrophoretic mobility shift assay using a probe specific for NF-κB. Arrows indicate the induced NF-κB complex. **b**, Peritoneal macrophages were stimulated with LPS (left), MALP-2 (middle) or R-848 (right) for 10 or 20 min. Whole-cell lysates were prepared and subjected to western blot analysis using antibodies specific for the indicated molecules. **c**, Lysates from macrophages stimulated with LPS (left), MALP-2 (middle) or R-848 (right) were immunoprecipitated with antibodies against IRAK-1. The kinase activity of IRAK-1 was measured by *in vitro* kinase assay (top). The same lysates were blotted with antibodies against IRAK-1 (bottom). Auto indicates auto-phosphorylation.

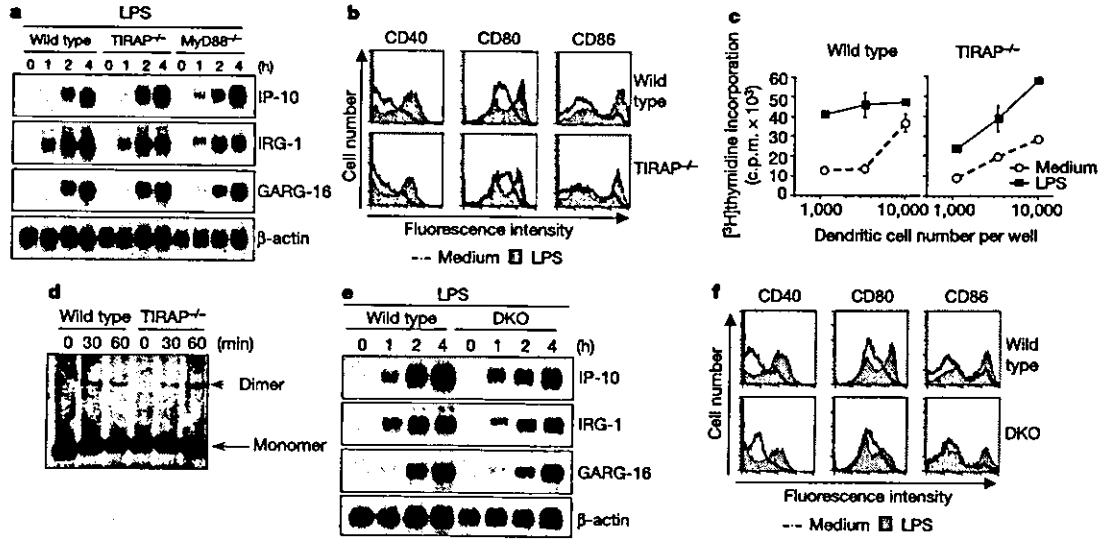


**Figure 5** LPS-induced activation of the MyD88-independent signalling pathway in TIRAP-deficient mice. **a**, Peritoneal macrophages were stimulated with 1 ng ml$^{-1}$ LPS for the indicated durations. Total RNA (5 μg) was extracted and subjected to northern blot analysis for expression of genes encoding IP-10, IRG-1 and GARG-16. The same membrane was re-hybridized with a β-actin probe. **b**, Bone-marrow-derived dendritic cells were stimulated with 100 ng ml$^{-1}$ LPS for 24 h and analysed for surface expression of the indicated molecules by flow cytometry. **c**, LPS-stimulated (squares) or unstimulated (open circles) bone-marrow-derived dendritic cells (H-2$^b$) were irradiated and incubated with allogeneic BALB/c CD4$^+$ T cells (H-2$^d$) at the indicated concentrations. Proliferative responses of T cells were evaluated by the [$^3$H]thymidine incorporation of CD4$^+$ T cells. **d**, Peritoneal macrophages were stimulated with 1 μg ml$^{-1}$ LPS for 30 or 60 min. Cell lysates were prepared and resolved by native PAGE. Monomeric (arrow) and dimeric (arrowhead) forms of IRF-3 were detected by western blot. **e**, Peritoneal macrophages from wild-type and MyD88, TIRAP doubly deficient mice (DKO) were stimulated with LPS and analysed for the expression of IP-10, IP-10, IRG-1 and GARG-16 by northern blotting. **f**, Bone-marrow-derived dendritic cells from wild-type and MyD88, TIRAP doubly deficient mice (DKO) were cultured with 100 ng ml$^{-1}$ LPS for 24 h. The surface expression of the indicated molecules was analysed by flow cytometry.

TIRAP is involved in the LPS-induced activation of the MyD88-independent pathway[8,9,16,17]. We therefore examined whether TIRAP deficiency affects the MyD88-independent signalling. Peritoneal macrophages from wild-type, TIRAP-deficient and MyD88-deficient mice were stimulated with LPS and analysed for the induction of IFN-inducible genes encoding IP-10, GARG-16 and IRG-1 by northern blot analysis (Fig. 5a). LPS induction of IP-10, GARG-16 and IRG-1 was comparable in wild-type, TIRAP-deficient and MyD88-deficient macrophages, indicating that the LPS induction of IFN-inducible genes was not impaired in TIRAP-deficient mice. LPS stimulation of wild-type dendritic cells (DCs) enhanced the expression of MHC class II and co-stimulatory molecules such as CD40, CD80 and CD86 (Fig. 5b). Similarly, TIRAP-deficient DCs showed enhancement of these surface molecules in response to LPS. In addition, LPS stimulation led to enhanced allo-stimulatory activity of DCs in both wild-type and TIRAP-deficient mice, showing that the LPS-induced maturation of DCs is retained in TIRAP-deficient mice, as it is in MyD88-deficient mice (Fig. 5c).

Because IRF-3 is reportedly activated in a MyD88-independent manner in response to LPS[7], we analysed the LPS-induced activation of IRF-3. When wild-type macrophages were stimulated with LPS, IRF-3 was activated and formed homodimers, as assessed by native polyacrylamide gel electrophoresis (PAGE) analysis (Fig. 5d). The LPS-induced dimerization of IRF-3 was similarly observed in TIRAP-deficient macrophages. Thus, the LPS-induced activation of IRF-3 is not affected in the absence of TIRAP.

These results did not exclude the possibility that MyD88 might compensate for the TIRAP deficiency and vice versa during the LPS response. We therefore generated mice lacking both MyD88 and TIRAP. Genes encoding IP-10, IRG-1 and GARG-16 were induced normally in response to LPS in the MyD88, TIRAP doubly deficient macrophages (Fig. 5e), and LPS-induced expression of co-stimulatory molecules was observed normally in MyD88, TIRAP doubly deficient DCs (Fig. 5f). Taken together, these findings indicate that TIRAP may not be essential for the LPS-induced activation of the MyD88-independent pathway.

We have examined the functional role of TIRAP by gene targeting. Our results do not support a model in which TIRAP is responsible for the TLR4-specific MyD88-independent events in TLR4 signalling, including the induction of IFN-inducible genes and the maturation of dendritic cells[8,9,16,17]. Instead, TIRAP has a role similar to that of MyD88 in TLR signalling. But the function of TIRAP seems to be confined to TLR4 and TLR2 signalling, which is distinct from the role of MyD88 as a common adaptor. Both MyD88 and TIRAP are essential to the common signalling pathway shared by TLR2 and TLR4, which leads to activation of IRAK-1 and NF-κB, and finally to cytokine production. There might be additional adaptors involved in the signalling pathway through other TLR members, as well as in the LPS-stimulated MyD88-independent pathway. Identification of such molecules will be important to our understanding of the molecular mechanism of the specific biological effects elicited by individual TLRs. □

## Methods

### Generation of TIRAP-deficient mice

Genomic DNA containing the mouse *Tirap* gene was isolated from 129/SV mouse genomic library and characterized by restriction enzyme mapping and sequencing analysis. We constructed the targeting vector by replacing a 1.6-kb fragment encoding a part of TIR domain with a *neo*$^R$ cassette, and inserted a herpes simplex virus thymidine kinase driven by the MC1 promoter into the genomic fragment for negative selection (Fig. 1a). The targeting vector was transfected into embryonic stem cells (E14.1) G418 and gancyclovir doubly resistant colonies were selected and screened by PCR and Southern blotting. We micro-injected homologous recombinants into C57BL/6 female mice and intercrossed heterozygous $F_1$ progenies to obtain TIRAP-deficient mice. TIRAP-deficient mice and their wild-type littermates from these intercrosses were used for experiments.

### Reagents

We purchased LPS from *Salmonella minnesota Re 595* prepared by a phenol/chloroform/petroleum ether extraction procedure from Sigma, PGN from *S. aureus* from Fluka, and poly(I:C) from Amersham. MALP-2 was synthesized and purified as described[14]. R-848 was a gift from the Pharmaceuticals and Biotechnology Laboratory of the Japan Energy Corporation. We prepared CpG oligodeoxynucleotides as described[11]. The polyclonal antibody against TIRAP was obtained by immunizing rabbit with bacterially expressed His-tagged full-length murine TIRAP protein. Antibodies against phosphorylated ERK, JNK and p38 were purchased from Cell Signaling. Antibodies against ERK, JNK and p38 were from Santa Cruz.

### Electrophoretic mobility shift assay

Peritoneal macrophages ($1 \times 10^6$) were stimulated with 100 ng ml$^{-1}$ LPS, 3 ng ml$^{-1}$ MALP-2 and 10 nM R-848 for the indicated durations. We purified nuclear extracts from cells and incubated them with a probe specific for the NF-κB DNA-binding site, separated them by electrophoresis and visualized them by autoradiography as described[10].

### Western blot analysis and *in vitro* kinase assay

Peritoneal macrophages were stimulated with 100 ng ml$^{-1}$ LPS, 3 ng ml$^{-1}$ MALP-2 or 100 nM R-848 for the indicated durations. The cells were then lysed in buffer containing 1.0% Nonidet-P40, 150 mM NaCl, 20 mM Tris-HCl (pH 7.5), 5 mM EDTA and protease inhibitor cocktail (Roche). We resolved the cell lysates by SDS–PAGE and transferred them onto a PVDF membrane (BioRad). The membrane was blotted with the indicated antibodies and visualized with an enhanced chemiluminescence system (NEN Life Science Product). We measured the IRAK-1 activity in cell lysates by *in vitro* kinase assay as described[18].

### Preparation and analysis of dendritic cells

Bone marrow cells from wild-type or TIRAP-deficient mice were cultured with 10 ng ml$^{-1}$ granulocyte–macrophage colony-stimulating factor for 6 d. Immature dendritic cells were collected and cultured in fresh medium in the absence or presence of 100 ng ml$^{-1}$ LPS for a further 24 h. We stained the dendritic cells first with biotinylated antibodies against CD40, CD80 or CD86 and then with phycoerythrin (PE)-conjugated streptavidin. We carried out flow cytometric analysis using a FACSCalibur with CELLQuest software (Becton Dickinson). The allo-stimulatory activity of dendritic cells was analysed as described[4].

### Native PAGE assay

Peritoneal macrophages were stimulated with 1 (μg ml$^{-1}$ LPS for the indicated periods and then lysed. The cell lysates in native PAGE sample buffer (62.5 mM Tris-HCl (pH 6.8), 15% glycerol and 1% deoxycholate) were separated by native PAGE and then immunoblotted with antibodies against IRF-3 as described[19].

Received 1 July; accepted 9 September 2002; doi:10.1038/nature01182.


1. Akira, S., Takeda, K. & Kaisho, T. Toll-like receptors: critical proteins linking innate and acquired immunity. *Nature Immunol.* **2**, 675–680 (2001).
2. Imler, J. L. & Hoffmann, J. A. Toll-like receptors in innate immunity. *Trends Cell Biol.* **11**, 304–311 (2001).
3. Medzhitov, R. Toll-like receptors and innate immunity. *Nature Rev. Immunol.* **1**, 135–145 (2002).
4. Janeway, C. A. Jr & Medzhitov, R. Innate immune recognition. *Annu. Rev. Immunol.* **20**, 197–216 (2002).
5. Kawai, T., Adachi, O., Ogawa, T., Takeda, K. & Akira, S. Unresponsiveness of MyD88-deficient mice to endotoxin. *Immunity* **11**, 115–122 (1999).
6. Kaisho, T., Takeuchi, O., Kawai, T., Hoshino, K. & Akira, S. Endotoxin-induced maturation of MyD88-deficient dendritic cells. *J. Immunol.* **166**, 5688–5694 (2001).
7. Kawai, T. *et al.* Lipopolysaccharide stimulates the MyD88-independent pathway and results in activation of IRF-3 and the expression of a subset of LPS-inducible genes. *J. Immunol.* **167**, 5887–5894 (2001).
8. Horng, T., Barton, G. M. & Medzhitov, R. TIRAP: an adapter molecule in the Toll signaling pathway. *Nature Immunol.* **2**, 835–841 (2001).
9. Fitzgerald, K. A. *et al.* Mal (MyD88-adaptor-like) is required for Toll-like receptor-4 signal transduction. *Nature* **413**, 78–83 (2001).
10. Adachi, O. *et al.* Targeted disruption of the MyD88 gene results in loss of IL-1- and IL-18-mediated function. *Immunity* **9**, 143–150 (1998).
11. Hemmi, H. *et al.* A Toll-like receptor recognizes bacterial DNA. *Nature* **408**, 740–745 (2000).
12. Hemmi, H. *et al.* Small anti-viral compounds activate immune cells via the TLR7-MyD88-dependent signaling pathway. *Nature Immunol.* **3**, 196–200 (2002).
13. Alexopoulou, L., Holt, A. C., Medzhitov, R. & Flavell, R. A. Recognition of double-stranded RNA and activation of NF-κB by Toll-like receptor 3. *Nature* **413**, 732–738 (2001).
14. Takeuchi, O. *et al.* Cutting edge: preferentially the R-stereoisomer of the mycoplasmal lipopeptide macrophage-activating lipopeptide-2 activates immune cells through a toll-like receptor 2- and MyD88-dependent signaling pathway. *J. Immunol.* **164**, 554–557 (2000).
15. Takeuchi, O. *et al.* Differential roles of TLR2 and TLR4 in recognition of Gram-negative and Gram-positive bacterial cell wall components. *Immunity* **11**, 443–451 (1999).
16. Toshchakov, V. *et al.* TLR4, but not TLR2, mediates IFN-β-induced STAT1α/β-dependent gene expression in macrophages. *Nature Immunol.* **3**, 392–398 (2002).
17. O'Neill, L. A. Toll-like receptor signal transduction and the tailoring of innate immunity: a role for Mal? *Trends Immunol.* **23**, 296–300 (2002).
18. Sato, S. *et al.* A variety of microbial components induce tolerance to lipopolysaccharide by differentially affecting MyD88-dependent and -independent pathways. *Int. Immunol.* **14**, 783–791 (2002).
19. Iwamura, T. *et al.* Induction of IRF-3/-7 kinase and NF-κB in response to double-stranded RNA and virus infection: common and unique pathways. *Genes Cells* **6**, 375–388 (2001).


**Supplementary information** accompanies the paper on *Nature*'s website (http://www.nature.com/nature).

**Acknowledgements** We thank P. F. Mühlradt and H. Tomizawa for MALP-2 and R-848, respectively; E. Horita for secretarial assistance; and N. Okita and N. Iwami for technical assistance. This work was supported by grants from Special Coordination Funds, the Ministry of Education, Culture, Sports, Science and Technology, and Research Fellowships from the Japan Society for the Promotion of Science for Young Scientists.

**Competing interests statement** The authors declare that they have no competing financial interests.

**Correspondence** and requests for materials should be addressed to S.A. (e-mail: sakira@biken.osaka-u.ac.jp).

# The adaptor molecule TIRAP provides signalling specificity for Toll-like receptors

**Tiffany Horng, Gregory M. Barton, Richard A. Flavell & Ruslan Medzhitov**

*Howard Hughes Medical Institute, Section of Immunobiology, Yale University School of Medicine, New Haven, Connecticut 06520, USA*

**Mammalian Toll-like receptors (TLRs) function as sensors of infection and induce the activation of innate and adaptive immune responses[1–3]. Upon recognizing conserved pathogen-associated molecular products, TLRs activate host defence responses through their intracellular signalling domain, the Toll/interleukin-1 receptor (TIR) domain, and the downstream adaptor protein MyD88 (refs 1–3). Although members of the TLR and the interleukin-1 (IL-1) receptor families all signal through MyD88, the signalling pathways induced by individual receptors differ. TIRAP, an adaptor protein in the TLR signalling pathway, has been identified and shown to function downstream of TLR4 (refs 4, 5). Here we report the generation of mice deficient in the *Tirap* gene. TIRAP-deficient mice respond normally to the TLR5, TLR7 and TLR9 ligands, as well as to IL-1 and IL-18, but have defects in cytokine production and in activation of the nuclear factor NF-κB and mitogen-activated protein kinases in response to lipopolysaccharide, a ligand for TLR4. In addition, TIRAP-deficient mice are also impaired in their responses to ligands for TLR2, TLR1 and TLR6. Thus, TIRAP is differentially involved in signalling by members of the TLR family and may account for specificity in the downstream signalling of individual TLRs.**

Studies have established the TLR family as the essential recognition and signalling component of mammalian host defence[1–3]. Ten mammalian TLRs have been described so far, and microbial ligands for many of them have been identified. TLR ligands represent molecular products derived from all of the main classes of pathogens and include the TLR4 ligand lipopolysaccharide (LPS)[6], the TLR3 ligand double-stranded RNA[7], the TLR2 ligands peptidoglycan (PGN)[8] and bacterial lipoproteins[9–11], the TLR5 ligand flagellin[12], and the TLR9 ligand unmethylated CpG DNA[13]. Synthetic ligands for TLR7, imiquimod and resiquimod (R-848), have also been described[1]. Understanding the functional differences between individual TLRs, especially in terms of signalling pathways and cellular responses induced by various microbial ligands, is a subject of great interest[3,14].

The adaptor protein TIRAP may be responsible for differential signalling by individual TLRs[4,5]. A dominant-negative form of TIRAP inhibits the activation of nuclear factor NF-κB induced by TLR4, but not by TLR9 or the interleukin 1 receptor (IL-1R)[4]. Consistent with this, TIRAP interacts with TLR4 but not with TLR9 in glutathione *S*-transferase pull-down assays. On the basis of these results, we considered that TIRAP might be responsible for the cellular responses that can be observed in MyD88-deficient cells stimulated by LPS but not CpG. Specifically, although LPS-stimulated MyD88-deficient dendritic cells (DCs) can no longer make cytokines, they still retain the ability to upregulate the co-stimulatory molecules CD80 and CD86 (ref. 15). In addition, NF-κB and mitogen-activated protein (MAP) kinases are still activated, albeit with delayed kinetics, in MyD88-deficient macrophages[16,17]. Similar to TLR9, TLR2 is thought to lack signalling through the MyD88-independent pathway, because macrophage-activating lipopeptide 2Kd (MALP-2), a ligand for the TLR2–TLR6 receptor pair, does not activate NF-κB in MyD88-deficient macrophages[16].

To characterize the role of TIRAP in innate immunity, we generated TIRAP-deficient mice by homologous recombination. Embryonic stem (ES) cells were electroporated with the targeting vector, in which a 640-base-pair (bp) exon encoding most of the coding sequence of the *Tirap* gene was replaced with the neomycin resistance (*neo*$^R$) cassette (Fig. 1a). Two independently derived, correctly targeted ES cell clones (Fig. 1b) were then microinjected into C57BL/6 blastocysts. Chimaeric pups were bred to female C57BL/6 mice, and transmission of the mutated allele was monitored by Southern blot analysis of genomic DNA from the offspring (data not shown). Heterozygous mice were then interbred to produce offspring homozygous for the *Tirap* deletion (Fig. 1c). TIRAP-deficient mice were born at the expected mendelian ratio and showed no obvious gross abnormalities. Experiments were done with both knockout lines and similar results were obtained. The absence of TIRAP mRNA was verified by polymerase chain reaction with reverse transcription (RT–PCR) analysis of RNA isolated from the knockout mice (Fig. 1d).

We first looked at the effects of the *Tirap* deletion in B cells. Splenocyte proliferation was measured in response to the TLR4 ligand LPS, the TLR7 ligand R-848, the TLR9 ligand CpG and tripalmitoyl cysteinyl (Pam3Cys) lipopeptide (bacterial lipopeptide; BLP), which signals through the TLR1–TLR2 heterodimer[18].

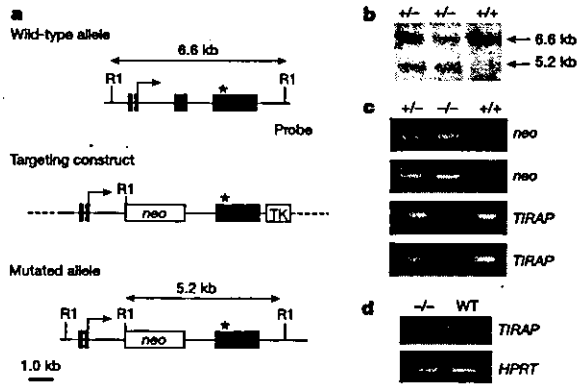


**Figure 1** Generation of TIRAP-deficient mice. **a**, The mouse *Tirap* gene, the targeting vector and the mutated allele. Filled boxes denote exons, and the arrow and the asterisk mark the AUG translation start site and the stop codon, respectively. 'RI' marks the *Eco*RI sites used for Southern blot analysis. TK, thymidine kinase gene. **b**, Southern blot analysis of *Eco*RI-digested genomic DNA from the two injected ES cell clones (left and middle) and a wild-type ES cell clone (right). **c**, PCR of genomic tail DNA from homozygous knockout (−/−), heterozygous (+/−) and homozygous wild-type (+/+) mice using two combinations each of primers that detect the *neo*$^R$ gene (top two panels) and the deleted exon (bottom two panels). **d**, RT–PCR of cDNA from TIRAP-deficient and wild-type (WT) littermates indicate the absence of TIRAP mRNA in TIRAP-deficient cells (top). Amplification of *HPRT* cDNA was included as a control (bottom).

  